UNCLASSIFIED

SECURITY CLASSIFICATION OF THIS PAGE (When Data Entered)

REPORT DOCUMENTATION PAGE

READ INSTRUCTIONS BEFORE COMPLETING FORM

1. REPORT NUMBER: AFOSR-TR- 82 -0217
2. GOVT ACCESSION NO.: AD-A114753
3. RECIPIENT'S CATALOG NUMBER:

4. TITLE (and Subtitle): NEW APPROACHES TO OPTICAL SYSTEMS FOR INERTIAL ROTATION SENSING
5. TYPE OF REPORT & PERIOD COVERED: Interim Scientific Report 1-1-80 through 12-31-80
6. PERFORMING ORG. REPORT NUMBER: G. L. 3341

7. AUTHOR(s): M. Chodorow, C. C. Cutler, S. A. Newton, G. A. Pavlath, and H. J. Shaw

8. CONTRACT OR GRANT NUMBER(s): F49620-80-C-0040

9. PERFORMING ORGANIZATION NAME AND ADDRESS: Stanford University, Edward L. Ginzton Laboratory, Stanford, California 94305

10. PROGRAM ELEMENT, PROJECT, TASK AREA & WORK UNIT NUMBERS: 61102F 2301/A1

11. CONTROLLING OFFICE NAME AND ADDRESS: Director of Electronic and Material Sciences, Air Force Office of Scientific Research, Attn: NE, Building 410, Bolling AFB, D.C. 20332

12. REPORT DATE: December 1981

13. NUMBER OF PAGES: 88

14. MONITORING AGENCY NAME & ADDRESS (if different from Controlling Office):

15. SECURITY CLASS. (of this report): UNCLASSIFIED

15a. DECLASSIFICATION DOWNGRADING SCHEDULE:

16. DISTRIBUTION STATEMENT (of this Report)

Approved for public release; distribution unlimited.

17. DISTRIBUTION STATEMENT (of the abstract entered in Block 20, if different from R...)

18. SUPPLEMENTARY NOTES

19. KEY WORDS (Continue on reverse side if necessary and identify by block number)

Sagnac rotation sensor (reentrant, pulsed operation of)
Fiber optic components
Directional coupler
Polarizer
Polarization controller
Rayleigh scattering (in optical fibers)
Polarization in optical fibers
Jones matrices

20. ABSTRACT (Continue on reverse side if necessary and identify by block number)

The objective of this research program has been to investigate the potential of new fiber optic configurations for inertial rotation sensing so as to extend the sensitivity and stability of such systems. In particular, the research has been aimed at the design and construction of reentrant Sagnac systems permitting recirculation of the optical signals.

There have been two main activities in the program, (1) the design and partial construction of an all-fiber Sagnac rotation sensor eliminating all previously

DD FORM 1473

used bulk optical components, lenses, mirrors, prisms, etc. Bulk components do not have sufficient precision and impose alignment problems so as to limit the sensitivity and recirculation capability of Sagnac sensors. The all fiber design was made possible by the development in this laboratory partially under other contract support of a set of all fiber components, directional couplers, polarizers, and polarization controllers, which have been incorporated in the all fiber design. This configuration should provide greatly increased sensitivity and device compactness and ruggedness. The second set of activities in the program has been to investigate various limitations on the sensitivity (minimum detectable rotationrate) of Sagnac systems. One such limitation is the extraneous noise known to exist in all Sagnac systems. We have found particularly, that the effects of Rayleigh backscattering from fiber inhomogeneities of phase detection in Sagnac systems, as one of the principle limitations on sensitivity. Investigation of various possible means of circumventing this very fundamental noise source are underway. The second major effect on Sagnac sensitivity comes from signal polarization and the effects of fiber properties on polarization conversion along the fiber path. A detailed mathematical formalism has been developed to treat the effects of polarization conversion on ultimate Sagnac sensitivity. As a result of this mathematical treatment, a particular form of source polarization and a specific set of operating conditions for a Sagnac sensor has been suggested which should minimize the deleterious effects of polarization conversion. This configuration has been tested and has worked quite successfully.

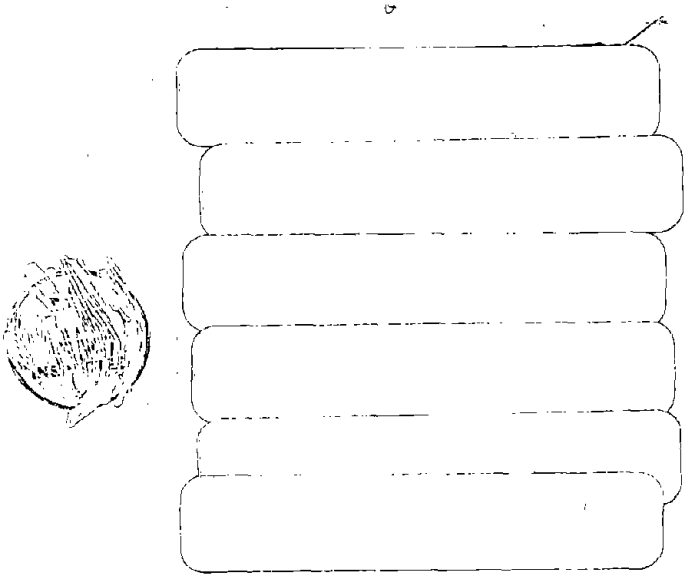

DISCLAIMER NOTICE

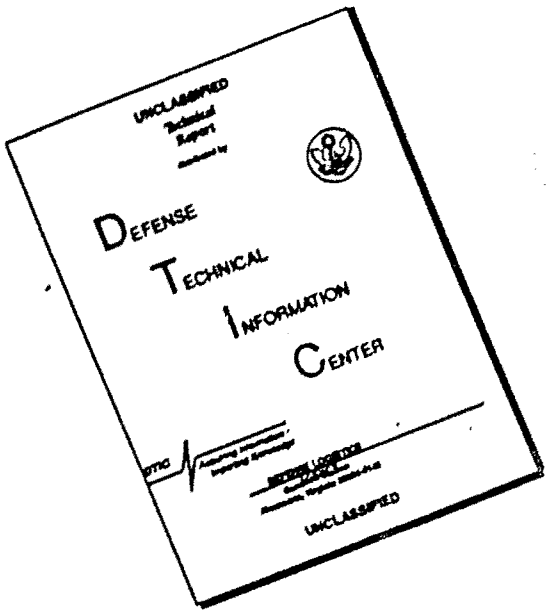

THIS DOCUMENT IS BEST QUALITY AVAILABLE. THE COPY FURNISHED TO DTIC CONTAINED A SIGNIFICANT NUMBER OF PAGES WHICH DO NOT REPRODUCE LEGIBLY.

F49620-80-C-0040

TABLE OF CONTENTS

Approved for public release;
Distribution unlimited

I. INTRODUCTION

A. OBJECTIVE

The objective of this research program has been to investigate the potential of new fiber optic configurations for inertial rotation sensing, so as to extend the sensitivity and basic stability of such systems. The approach has involved basic device research, including both theoretical analysis and experimental demonstrations for the purpose of improving future generations of operational rotation sensing systems. We have introduced new concepts in the use of optical fibers in rotation sensing loops, specifically the recirculation of optical pulses in these loops (reentrant Sagnac system), and eventually active operation of these loops (i.e., the incorporation of an amplifier in the loop), aimed at increasing the sensitivity, stability, and optical integration times of these devices by very large factors.

B. PROGRAM SUMMARY

This program has had two main sets of activities over the past year. The first was concerned with continuation of the previous work under the AFOSR, aimed at the design and construction of an active reentrant Sagnac (ARS) pulsed all-fiber optic system for inertial rotation sensing. This system is described in Section II. The current phase of the work is leading to a passive all-fiber reentrant system (PRS). There are no all-fiber reentrant gyros of any kind in existence at this time, to our knowledge.

The second activity has been concerned with examining various problems related to the sensitivity (minimum detectable rotation rates) of Sagnac

systems. R & D on devices in which CW light waves make a single pass round a multi-turn fiber optic sensing loop is being carried on in a number of laboratories. At the start of the present reporting period, all such devices were limited to sensitivities far below theoretical predictions and there was an urgent need to overcome these noise barriers. This problem became an important part of our activity. In this, we are largely concerned with studying the effects of various sources of noise in the fiber and the effects of birefringence and nonreciprocity in the fiber.

Our activity on these two sets of problems is described briefly below and in greater detail in the body of this report (Section II on Recirculating Sagnac System and Section III on New Techniques for Fiber Gyroscopes).

Obviously methods for increasing the sensitivity and accuracy in the measurement of extremely small rotation rates are of great importance to Air Force objectives in the fields of inertial navigation and geodesy. It is also relevant to point out that fiber sensors are growing increasingly important for measuring a variety of environmental effects including strain, acoustic waves, current, magnetic field, temperature and so forth as well as inertial rotation. Typically, such devices require fiber interferometers for measuring small optical phase shifts, and these interferometers all require single mode fibers. Consequently, any research on fiber rotation sensors in our present program and the developing of components will lead to new techniques for single mode fiber systems which are important for these other sensors. The results also may be of importance for signal processing systems and communications systems of the future.

C. REVIEW OF CURRENT ACTIVITIES

The ultimate objective of the program is an active system incorporating an amplifier in the rotation sensing loop. Our activity up to now, however, has involved rotation sensing by passive operation of pulsed recirculating fiber optic loops, or passive reentrant Sagnac systems (PRS), that is, with no amplifier. Using standard optical bench components it has been possible, prior to this reporting period, to observe five recirculation pulses in the fiber loop. Such operation multiplies the effective length of the fiber by the number of recirculations and increased the rotation sensitivity of the system in accord with the theory. All this refers to PRS operation as described above where the system is operated in a recirculating mode but passively. These results showed that standard optical bench components do not have sufficient precision to align the system for simultaneous optimum pulse recirculation and rotation sensitivity. It is possible that more precise optical components could overcome these problems and improve performance. However, our experience indicates the required precision and quality would be difficult to achieve. More important, however, we have developed a much superior and simpler approach which will be described below.

In principle the mode and alignment problems with bulk recirculating components could be completely circumvented by the use of integrated (single mode) fiber components. No such components with sufficiently high performance and low enough loss were available when the program was started. Subsequently, however, under a companion program (JSEP) in the laboratory concerned with optical signal processing, we developed single mode fiber optic

directional couplers which appear to satisfy all the requirements for a PRS. In addition, other fiber components, polarizers, polarizer controllers and so on have been also developed under another contract and these eliminate all the mode and alignment problems encountered with hybrid systems. They provide miniaturization, ruggedness and decreased system expense. We have designed and tested various components and sub-systems to be incorporated into an all-fiber recirculating system. Because of the unavailability of some particular optimum fibers we were not able to complete the system, but the design is completed and the fabrication was well along by the end of the reporting period. These various components, the design of the system and expected performance are described in Section II below.

It is perhaps useful to mention here that such components have been incorporated in a CW nonrecirculating Sagnac system. The system and the components have operated very satisfactorily and have given higher sensitivity in rotation sensing than anything else that has been achieved in a fiber system. It must be emphasized, again however, that this is not a recirculating system which limits its ultimate sensitivity. This was done under the auspices of another contract, but has provided very useful design information and operating experience which is very relevant to the pulsed recirculating system which is now under construction under this program. Conversely many of the design features and operating characteristics of this CW Sagnac system are based on data and insights gained from other AFOSR work on recirculating systems. The existence of both programs in the laboratory with different objectives has been of great mutual benefit.

As to the second set of activities referred to above, which are concerned with sensitivity, basically we have worked in two main areas. One dealt with a previously unsuspected major source of noise in the systems. This is Rayleigh scattering from inhomogeneities in the fiber which produces a noise level much higher than the previously estimated theoretical lower limits. This work is discussed in further detail in Section III, including various approaches we have developed to reduce this noise which we are now investigating under the continuation of the contract. The proposed experiments will integrate well with the work on the recirculating rotation sensor since the experimental facility being built is ideally suited for testing some of these new ideas. The second major problem related to the ultimate sensitivity of fiber rotation sensors arises from the effects of birefringence and the coupling between the two orthogonal polarizations in a single mode fiber. We had previously pointed out the importance of polarization and, in particular, the importance of reciprocity in operation of fiber rotation sensors and we have now developed a mathematical formalism which can treat birefringence effects in a most general way, including environmental effects which are important both for the Rayleigh scattering and for the cross talk between two polarization channels. As a result of this theoretical analysis we have developed the idea that a fiber rotation sensor using unpolarized light, that is, with no correlation between the two orthogonal polarization channels, could lead to greater sensitivity in a gyro. In the body of the report the details of the formalism we have developed to treat birefringent effects and the measured properties of such an unpolarized gyro are described. These ideas are being pursued further under the continuing contract.

II. PASSIVE RECIRCULATING SAGNAC SYSTEM

A. SUMMARY OF PROGRESS DURING REPORTING PERIOD

The work on the passive recirculating Sagnac (PRS) system during the reporting period has been concerned with design and construction of a new system. This new system features the use of all-fiber components in the sensing loop and interferometer.

The new design is based on the results obtained under the program during the preceding year, which validated the basic mechanisms of the PRS system. That system employed hybrid, bulk-optic components and unguided optical beams in space for all portions of the system except for the sensing loop proper. As shown in the report for that period[1] that first system, in addition to serving the purpose of establishing the basic principle, also demonstrated clearly the non-feasibility of pursuing recirculating systems further with bulk optics components.

In addition to their obvious size, cost and stability disadvantages, bulk components also suffer from multimoding and alignment problems, and the experience with the first system made it clear that simultaneous alignment for efficient injection, balanced counter-propagating wave amplitudes, and low loss recirculation, involved mutually interacting adjustments which were extremely difficult to program, carry out, and stabilize. It also became clear that all-fiber, all-single mode components should completely circumvent all of these problems.

---

[1] Final Report for Grant No. AFOSR-76-3070, "Research on New Approaches to Optical Systems for Inertial Rotation Sensing," Edward L. Ginzton Laboratory Report No. 3094, Stanford University (February 1980).

The bulk-optics version was constructed at a time when no all-fiber components existed. The need for such components for the PRS system was the initial driving force for a program here which resulted in the development of components of this kind. It was realized that such components would have wide applicability to other programs both here and elsewhere, for general signal processing devices using optical fibers. The first of such single-mode fiber devices, a directional coupler, was developed under Joint Services support (JSEP) and this was followed by subsequent development of a polarizer, which used the basic coupler format, and a polarization controller, both under industrial support from Atlantic Richfield Company. The designs and fabrication techniques for these components are now established and are available to the present program for use in an all-fiber PRS system.

During the reporting period, we suffered from a materials problem. We have switched from a jacketed fiber (ITT) used during the preceding year[1] to a new fiber (Corning). The purpose was to change from the visible light (HeNe) used in the bulk-optic system to near IR light (Nd:YAG). This change had the advantages of lower propagation loss for the sensing loop and direct compatibility with the Nd:YAG single crystal fiber amplifier being developed under another program, and which will be used to convert the PRS system into an active recirculating system (ARS).

The Corning fiber, although having the desired transmission characteristics at 1.06 μ wavelength, was unjacketed. No jacketed fiber designed for operation at that wavelength was available at that time. During the reporting period we did fabricate operational all-fiber components using that fiber. However, the fiber was found to be very difficult to work with. The procedures which were productive with jacketed fiber were not satisfactory for the unjacketed fiber, and the yield was low. Also, fiber-to-fiber splices using

this fiber showed high insertion loss (several dB per splice), and the fabrication problems with this fiber made it non-feasible to attempt to fabricate multiple components on an unbroken fiber to avoid splices. Multiple components were successfully constructed in this way using the ITT jacketed fiber, for operation at .9 μ. This approach has important advantages for the PRS system because of the sensitivity to splice losses when the recirculating waves make multiple transits across the splices.

By the time this stage was reached, a jacketed fiber designed for operation in the 1.06 μ range became commercially available (Corning) and the decision was then made to change to the new fiber. This occurred near the end of the reporting period, and procurement was initiated at that time, with expectation of delivery in the first few months of the following period.

During the reporting period the design for the all-fiber PRS system was undertaken and completed. By the end of the period, techniques for fabrication of all components needed for the fiber portions of the system were on hand, and a new fiber was on order which was expected to allow fabrication of these components on a single unbroken strand of fiber. Design, procurement and construction activities for all other (non-fiber) portions of the new PRS system continued during the reporting period.

B. SYSTEM DESIGN

1. Basic Recirculating System

In the basic recirculating Sagnac system, shown in block form in Fig. 1, light from a pulsed source is sent, via an optical junction, into a multiturn fiber sensing loop, where it makes multiple circulations around

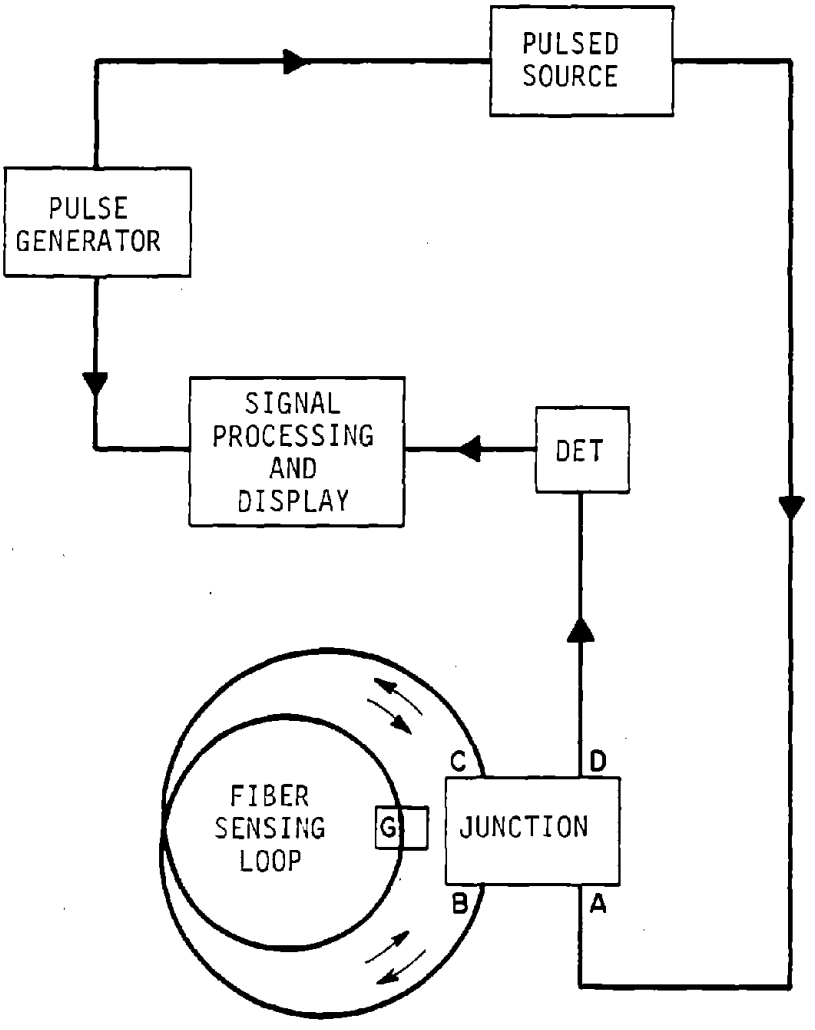

Fig. 1--Basic schematic of recirculating system.

the loop. The light recirculating in the loop is nondestructively sampled by the junction and sent to an optical detector and associated video signal processor and display which measure inertial rotation of the sensing loop about an axis perpendicular to its plane.

The junction has the property that light entering at A is split into two equal-amplitude parts at B and C, leading to waves propagating clockwise and counterclockwise, respectively, around the loop. It also has the property of closing the loop upon itself, so that light, once propagating around the loop, continues to do so in multiple transits. The junction also has the property that it couples a given portion of both counter-propagating light waves, recirculating in the loop, back out of the loop and sends them to the detector.

The phases of the light waves are measured after each transit of the waves around the loop. To facilitate this, the output of the laser is pulsed with a pulse width somewhat less than the optical transit time once around the complete loop. The loop is active, containing an optical amplifier and other elements (G in the figure) to conserve pulses circulating in the loop. The amplifier compensates for optical attenuation due to propagation loss in the loop, energy extracted by the junction in the sampling process, and any internal loss in the junction. This leads to a time sampled output waveform whose envelope is sinusoidal in time. Measurement of the frequency of this waveform provides a measure of the angular velocity of the system. This is an essentially linear system, and as such is free of mode locking phenomena experienced with ring laser gyros.

Consider a single pulse extracted from the laser, leading to two pulses traveling in the loop, one clockwise and the other counterclockwise. After

these pulses have travelled once around the N-turns of the loop, they are reintroduced into the loop for a second transit, and this process is repeated until a total of K transits have been completed. The amplifier in the loop allows a large number of recirculations K, for large integration time against the rotation, and sensitivity to small rotation rates.

Each time the pulses complete a transit around the loop, they are sampled, and these samples are combined and sent to the detector. As the original pulses continue to recirculate around the loop, they generate a train of pulse samples at the detector, as a function of time. It is important to emphasize that this entire train of output pulses results from one single pulse extracted from the laser. The effect of rotation is to shift the phases of the optical pulses circulating around the loop. The clockwise and counterclockwise pulses are shifted in phase in opposite directions by the rotation, so that after exposure to rotation they possess a difference in phase, or relative phase shift. This relative phase shift is proportional to the rotation rate and also proportional to the length of time the pulses have been exposed to the rotation. As the pulses continue to circulate around the loop, they accumulate phase shift $\Delta\emptyset(t)$ which increases linearly with time t. The detector is a phase detector whose output is sinusoidal in the argument $\Delta\emptyset(t)$. That is, for a fixed rotation rate, the output of the detector is a sinusoidal wave in time. The frequency of this sinusoidal waveform is the same as the beat frequency in a standard ring laser gyro (RLG).

We refer to the system just described as an active recirculating Sagnac system (ARS) because of the presence of the amplifier in the sensing loop. When operated as a passive recirculating system (PRS) without the amplifier,

the output pulse train is a damped sinusoid whose amplitude decreases experimentally with time.

2. All-Fiber Interferometer

The design for the optical junction in single-mode fiber form is shown in Fig. 2(b), where the terminals A, B, C, D correspond to those in Fig. 1. DC1 and DC2 are single-mode fiber directional couplers. DC1 is a 3 dB coupler which splits the light pulses entering at A into two equal amplitude pulses at E and F, which enter coupler DC2 at opposite ends. DC2 is a directional coupler with a coupling coefficient (coupling between B and C and between E and F) near unity. Thus a large fraction of the light at E and F returns to F and E, respectively, while a small fraction enters the loop to form counterclockwise and clockwise traveling pulses, respectively. Pulses once in the loop remain in the loop by crossing from one side of DC2 to the other following the path shown by the dashed arrow, with low insertion loss because of the high coupling coefficient between the two halves 1 and 2 of the coupler, and the low internal dissipative loss of the coupler.

Making high quality splices on single mode fibers is difficult because of the small core diameter. Commercially available multimode splicing equipment yields splice losses of 1-3 dB when used on single mode fibers. Single mode splicing equipment with splice losses of around 0.1 dB is not currently available. In order to determine base-line performance for recirculating systems, the junction of Fig. 2 is designed to be fabricated, together with the sensing loop, with no fiber splices required. This calls for coupler halves 1, 2, 3, and 4 to be fabricated directly on the ends of the single-mode fiber sensing loop as at (a) and then assembled as at (b).

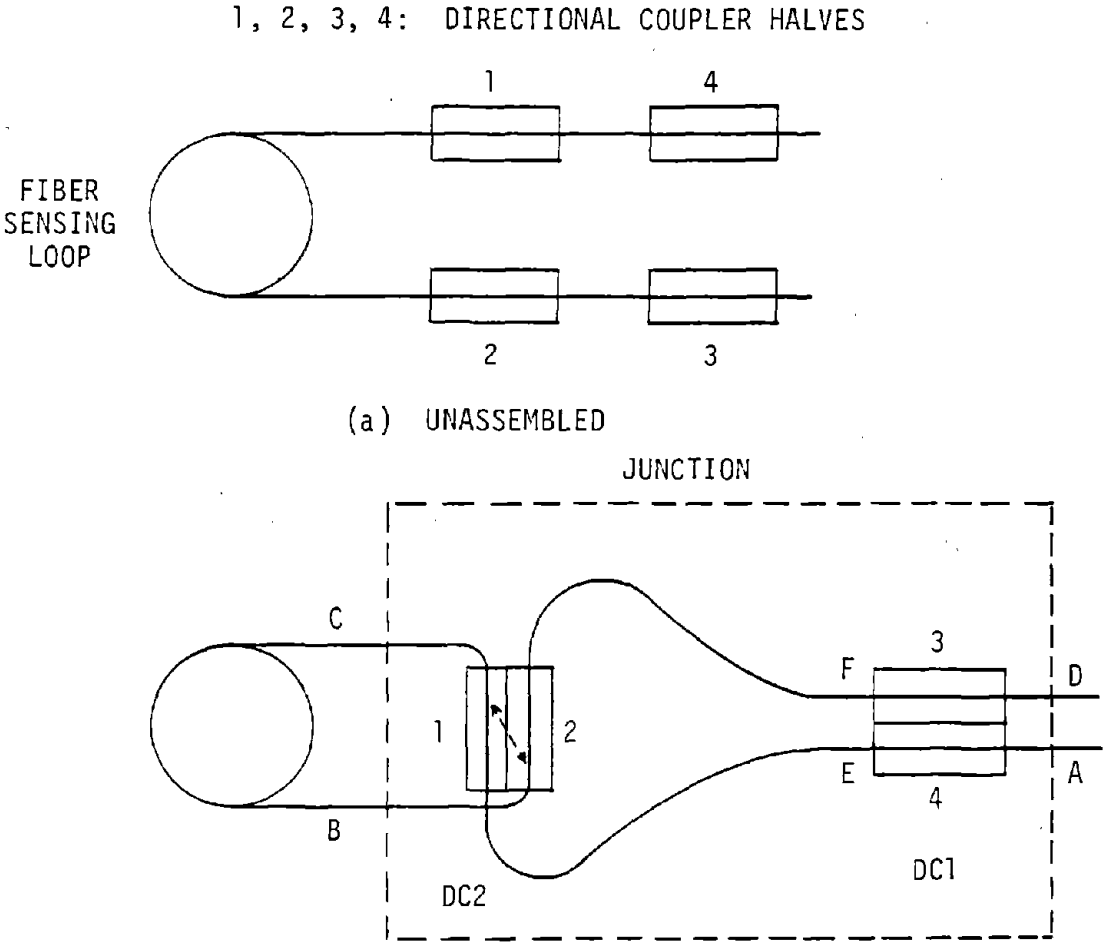

Fig. 2--Schematic for spliceless sensing loop and junction assembly.

3. Overall System

A diagram of the overall PRS system is given in Fig. 3. The system shown is passive, without an amplifier in the sensing loop, pending completion of a Nd:YAG fiber amplifier which is now under development in this laboratory under other auspices and will be added at a later date.

The optical source consists of a Nd:YAG laser operating at 1.06 μ, telescope, acousto-optic beam deflecting modulator, and beam steering device leading up to the fiber input.

Polarization controllers PC1 and PC2 are necessary to compensate the system for the birefringence in the fiber, in order to balance the interferometer at zero rotation rate.

Adjustments of the fiber circuit are expected to be simple and straightforward in sharp contrast to earlier models using bulk optic components within the interferometer. There are no optical alignments to be made within the interferometer.

C. COMPONENT DEVELOPMENT

The status of the various components in the circuit of Fig. 3 is discussed in this subsection.

1. Interferomter Components

Sensing Loop. The sensing loop will have a diameter of the order of 15 cm and will be wound with fiber having the following specifications:

Fiber type: single mode

Length ≅ 1 km

Core diameter = 6 μ

Cladding diameter = 125 μ

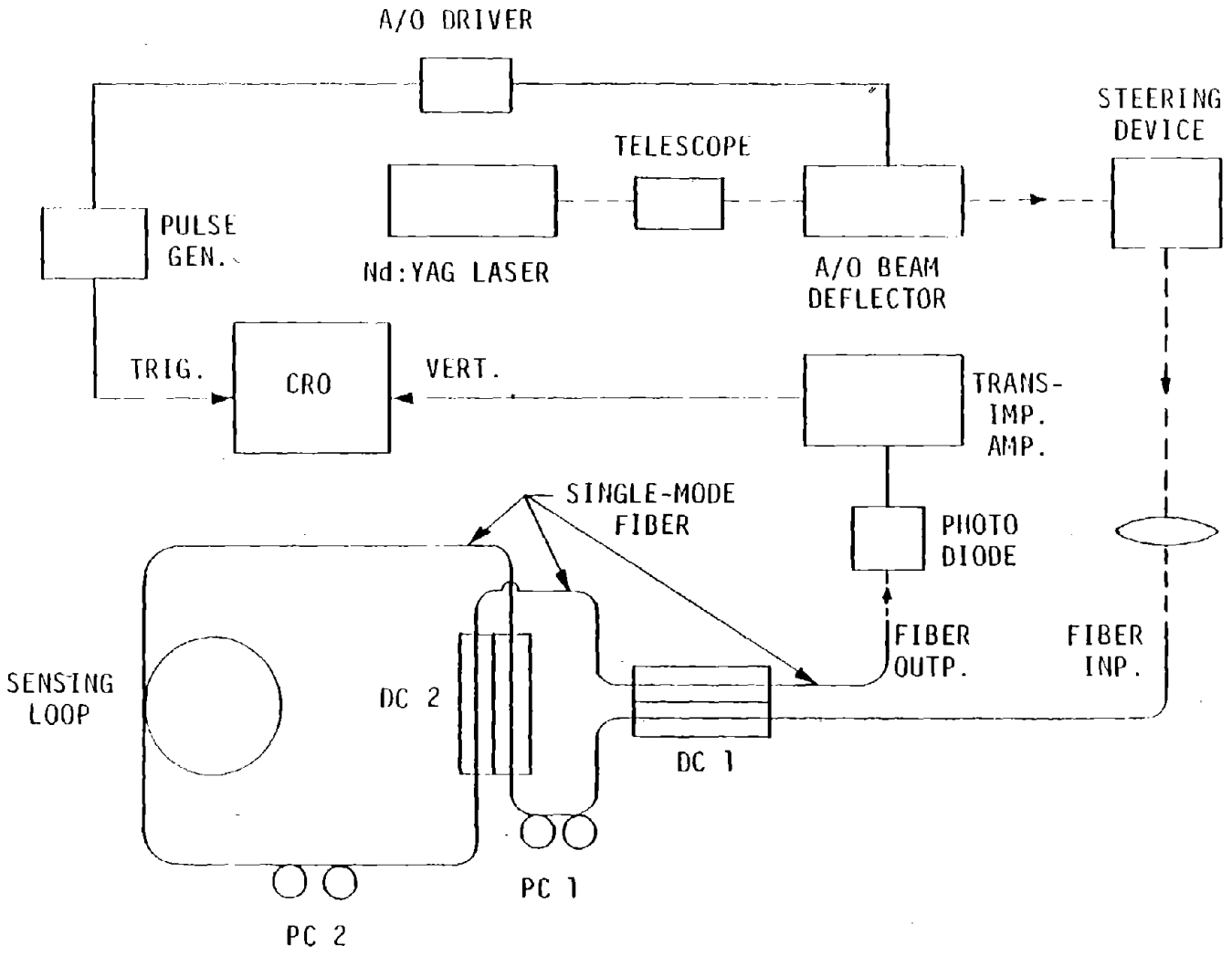

Fig. 3--Schematic for PRS system with all-fiber interferometer.

Optical attenuation (1.06 μ) ≅ 2 dB/km

Jacket diameter = 250 μ .

The loss in modern optical fibers is limited by Rayleigh scattering which varies inversely with the fourth power of the wavelength. To decrease this loss requires use of wavelengths in the near infrared. A wavelength of 1.06 μm was chosen because of the availability of powerful sources, the availability of fiber with loss of around 2 dB/km, and compatibility with a Nd:YAG amplifier under development. The sensing loop length was chosen to be 1 km because of the availability of fiber in that length and the high rotation sensitivity which it provides, and because with this length of fiber, pulses of several μs duration can be used which simplifies the equipment requirements for generation and detection of pulses.

Directional Couplers. A single-mode fiber-to-fiber, evanescent field directional coupler has been developed in this laboratory,[2] as noted above, and this design will be followed in fabricating the couplers DC1 and DC2 on the fiber just described. Briefly, in this coupler design, a fiber is bonded into a slot cut in a quartz substrate (Fig. 4a). The face of the block is polished to remove a significant portion of the cladding, thus allowing access to the evanescent fields of the guided mode (Fig. 4b). When two such substrates are placed in contact (Fig. 4c), strong coupling exists between the two fibers. This coupling is highly directional and can result in complete power transfer in approximately 1 millimeter of distance. The coupling can be varied by transverse displacement of the fibers (Fig. 4d).

---

[2] R. A. Bergh, G. Kotler, and H. J. Shaw, "Single-Mode Fibre Optic Directional Couplers," Electronics Letters 16, 7, 260 (27 March 1980).

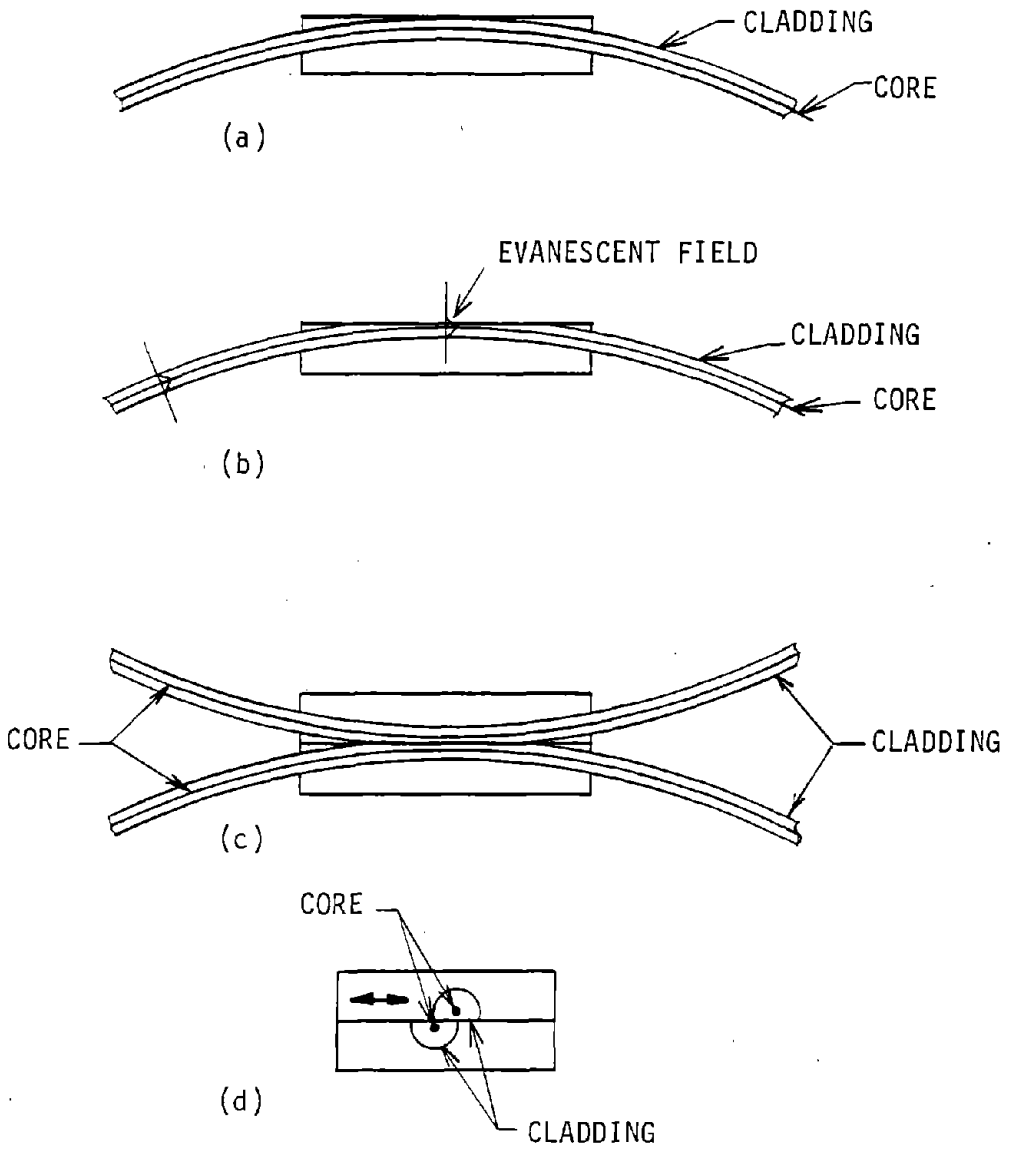

Figl 4--Fiber to fiber, evanescent field coupler. (a) Fiber bonded into slot cut in fused silica substrate. (b) Cladding partially removed to expose evanescent field. (c) Assembled coupler side view. (d) Tuning coupler (end view) by transverse displacement of blocks.

This coupler design is characterized by mechanically variable coupling coefficient, high directivity, low internal loss and low backscattering. Coupler DC-1 will be constructed with maximum coupling coefficient of 70%, which can then be set experimentally to 50% (3 dB coupler) during operation. Coupler DC2 will be constructed with slight over coupling at the maximum setting (interaction length > 1/2 wavelength), which can then be set experimentally to any desired value during operation. In the PRS system, there is an optimum value for this coupling coefficient k which maximizes the number n of observable pulses in the output pulse train, as n is given by

$$n = \frac{\ell n \frac{P_m}{P_0} + \ell n \frac{k}{(1 - k)^2}}{\ell N(kR)} \qquad (1)$$

where

P_0 = input power level

P_m = minimum detectable power level

R = power transmission coefficient of sensing loop = $\exp(-\alpha \ell)$ where α is the power attenuation coefficient of the fiber and ℓ is the fiber length.

For example, the optimum value of k varies from .975 to .75 as the fiber loss varies from 0 to 3 dB, and the corresponding value of n varies from 15 to 7. Thus a coupler which is capable of slight overcoupling can be tuned through this entire range, and set experimentally to match the attenuation constant of the particular fiber used, so as to maximize the number of recirculations.

For coupler DC2 the low internal loss in the present coupler design (measured < 0.5 dB) is crucial, as it is directly in series with the pulse recirculation path in the loop.

Polarization Controllers. The polarization controllers PC1 and PC2 (Fig. 3) are devices which can transform any state of polarization (in general elliptic with arbitrary ellipticity and axis orientation) at their input end to any other state of polarization at the output end. A design for this device[3] has been developed under another program in this laboratory. These controllers do not require any fiber splices, and do not involve any surgery on either the fiber or its jacket. They involve two small-diameter (1 or 2 cm depending on fiber characteristics) fiber loops whose bend-induced birefringence constitutes the equivalent of fractional-wave plates of very low loss, whose principle axes can be rotated experimentally to produce any desired transformation of the state of polarization.

2. External Components

This section discusses the components in Fig. 3 outside of the fiber circuit.

Laser. The external source is a General Photonics Model TWO-15, Ne:YAG laser operating at 1.06 μm. The power output is 2 watts in the TEM_{00} mode with a polarization of 1000:1. The $1/e^2$ beam diameter is 21 mm. The laser is equipped with a closed loop water-to-air heat exchanger, thus permitting the mounting of the entire laser system on the rotation table. The amplitude stability of the laser was measured at around 10%.

Pulse Modulator. An important design consideration is the requirement for a large number of recirculations. The ultimate limit on recirculations

[3] H. C. Lefevre, "Single-Mode Fibre Fractional Wave Devices and Polarisation Controllers," Electronics Letters 16, 20, 778 (25 September 1980).

is due to noise. In a poorly designed system, a significantly lower limit on recirculations can result from sensing loop round trip loss and finite modulation depth of the optical pulse generator. The non-zero power transmitted by the pulse generator in the interpulse period results in an optical background into which the recirculations decay because of sensing loop loss. The expected number of recirculations, n, is approximately given as

$$n = d/\alpha\ell \qquad (2)$$

where d is the modulation depth and $\alpha\ell$ is the total round trip loss in the sensing loop. For large n, Eq. (2) requires large modulation depths and/or low round trip losses. The round trip loss in the sensing loop has four components: loss in the optical fiber, splice losses, insertion loss of coupler DC2, and sampling loss. Sampling loss is due to coupling a nonzero amount of optical power from the sensing loop each recirculation for measurement of the accumulated Sagnac phase shift.

Based on the above considerations, the choice of an optical modulator was largely concerned with modulation depth capability. Q-switching the laser gives large modulation depths but also results in high peak powers which are not appropriate for use with single mode fiber operating in the linear range. In addition, the Q-switched pulses are narrow, which would require sophisticated detection equipment. An external modulator on a cw laser can give long pulses with low peak powers. Standard commercial modulators have modulation depths of 20-30 dB. For these modulators, Eq. (2) predicts 6 to 10 observable recirculations. Custom built systems could achieve around 45 dB of modulation depth but at a great increase in

price. Furthermore, this modulation depth is not as high as desired because it would limit the number of recirculations to 15 or less.

The pulse modulator shown in Fig. 5 was developed to provide modulation depths of better than 90 dB. The major components are an acousto-optic beam deflector, a coupling lens, and the optical fiber which functions as an apodized pinhole. This modulator functions as follows. When the acousto-optic beam deflector is on, the optical beam is deflected through an angle (θ), and the deflected beam is focused into the optical fiber by the coupling lens. The undeflected beam is focused a distance Δ away from the core of the fiber given by

$$\Delta = f\theta \qquad (3)$$

where f is the focal length of the coupling lens. For the values shown in Fig. 5, Δ is 106 μm. The spot size of the focused beam is around 3 μm, hence very little power from the undeflected beam is coupled into the fiber. The limit on the modulation depth is due to reflections from the surfaces of the coupling lens, and is 95 dB for an uncoated lens. For an AR coated lens the modulation depth can be increased to about 115 dB. Measurements of the modulation depth placed it at better than 46 dB. This measurement was limited by the sensitivity of the measurement system.

Reducing Telescope. A reducing telescope of reduction ratio 2.5 is used to match the laser beam to the acoustic aperture of the acousto-optic beam deflector.

Beam Deflector. A Coherent Model 304 acousto-optic beam deflector is used. The deflection angle is 7.1 mrads and the deflection efficiency was measured at 55% at a wavelength of 1.06 μm. The transmittance of the reducing telescope and beam deflector combination was measured to be 70% at 1.06 μm.

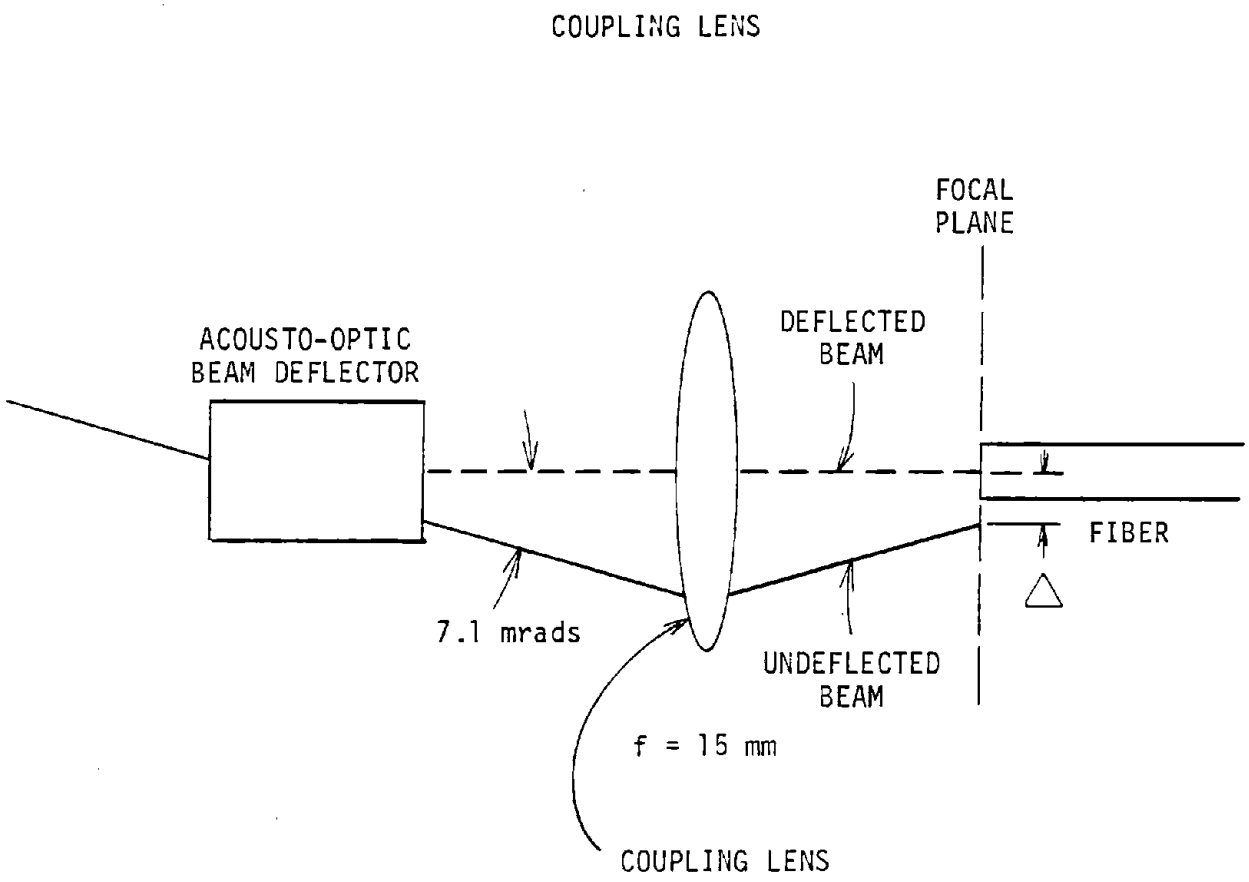

Fig. 5--Optical pulse generator with large modulation depth.

Steering Device. A model 605 beam steering device by Newport Research Corporation is used to steer the laser beam onto the coupling lens. The transmittance of this device is 99% at 1.06 μm.

Coupling Lens. A plano-convex lens of 15 mm focal lnegth is used. The coupling efficiency into the fiber was measured at 25%.

Photodiodes. Four types of photodiodes are available: A Centronics model OSD-1-4 IR enhanced silicon diode, a Centronics model APD-05-4, IR enhanced silicon avalanche diode, a Judsen Infrared model J-16-5 germanium diode, and a Ford Aerospace model L4520 low noise germanium diode.

Transimpedance Amplifiers. Three models are available from Judson Infrared: model 070, gain 50 dB, bandwidth 5 Hz-10 MHz; model 470, gain 26 dB, bandwidth 200 Hz-30 MHz, model 490, gain 26 dB, bandwidth 200 Hz-100 MHz.

Pulse Generator. An HP model 8013B pulse generator is used for the signal input into the acousto-optic driver. The pulse height is 5V, the pulse width 2 μs and the pulse period 200 μs. The pulse generator also provides a trigger signal for the oscilloscope.

Oscilloscope. An HP model 1742A, 100 MHz oscilloscope is used to display the measured pulse heights versus time. The bandwidth of the oscilloscope is user limited to 20 MHz to reduce noise.

III. NEW TECHNIQUES FOR FIBER GYROS

A. INTRODUCTION

All existing fiber gyros are based on the same mechanism, the Sagnac effect, in which EM waves traversing a closed path experience a phase shift proportional to the rate of rotation of the path in inertial space. All such gyros also use a multiturn sensing loop for the closed path, to multiply the phase shift and sensitivity. The various types of gyros differ only in the details of processing the optical signals inside and outside of the sensing loop, and the electrical signals from the detector, to emphasize various characteristics, such as sensitivity, dynamic range, response time, linearity, etc.

The sensitivity of fiber gyros is limited by instabilities and noise, of which quantum noise in the detector represents the irreducible minimum. As of the beginning of the reporting period, noise from other sources in excess of this minimum set the sensitivity limit of all existing fiber gyros.

We consider first effects of polarization. Earlier work under the present program[4] and elsewhere[5] had shown that reciprocity was a basic requirement for stable operation of fiber gyros of all types, i.e., that input and output polarizations of both counterpropagating pulses should be the same. This was the most significant advance since the inception of the fiber gyro, but it was clear that the subject was not closed, because only the case of linear polarization had been dealt with. Thus we turned to the development

---

[4] H. Arditty, H. J. Shaw, M. Chodorow, and R. Kompfner, Proc. Soc. Photo-Opt. Instrum. Eng. 157, 138 (1978).

[5] R. Ulrich and M. Johnson, Opt. Lett. 4, 5, 152 (1979).

of a formalism which would allow treating the general case of arbitrary polarization, as described in Sections III.B and C.

Much of the problem of increasing the sensitivity of fiber gyros is concerned with reducing noise resulting from residual environmental effects such as temperature changes and vibration which remain when the gyro is configured to be optically reciprocal. It is important to emphasize that every so-called single mode fiber is birefringent and actually supports two polarization modes. The birefringent effects are dependent upon environmental effects, and this leads to some of the instabilities and noise observed in fiber gyros. Sections III.B and C deal with the problem of handling these effects analytically. This analysis forms a very important guide to the process of reducing the noise and increasing the sensitivity of fiber gyros in general. This also has resulted in a proposal which is described below for a new form of gyro, using unpolarized light to achieve certain performance advantages.

Second, we consider the effects of light scattering. Initial theoretical work carried out under the present contract showed that coherent backscattering from random inhomogenieties in the fiber (Rayleigh scattering) is capable of reducing the sensitivity of fiber gyros to a level several orders of magnitude less than that imposed by photon noise, contrary to prior theoretical predictions. A discussion of this problem, including numerical estimates of the magnitude of the effect and general approaches for reducing it, is included below in Section III.D.

It is important to emphasize that Rayleigh scattering, as referred to above, is a property of all fibers in fixed amount, depending on the

wavelength. In Section III.D it is shown that even though this scattering is coherent, it leads to direct phase errors which, through the effects dealt with in Section III.B, are environmentally dependent, thus are non-systematic and cannot be calibrated, and must, therefore, be reduced in magnitude to acceptable levels. This work is expected to have a major impact in increasing the sensitivity of fiber gyros in general.

The analyses of Sections III.B, C and D are applied to single pass gyros using cw light. This is the simplest case and was the appropriate starting point. It has led to results of direct importance to practical gyros of this type which were under development in many laboratories. Extensions of this work to recirculating gyros of the type described in Section II will be treated in later reports.

B. BIREFRINGENCE EFFECTS

1. Introduction

The single mode optical fibers used in fiber optic gyroscopes are birefringent because they propagate two modes which have slightly different propagation constants. These two guided modes are the orthogonal polarizations of the HE_{11} mode. In an ideal fiber, the propagation constants of these modes would be identical. Small asymmetries enter into the fiber during the manufacturing process causing the fiber to be birefringent.

Intimately associated with birefringence is the polarization of the light which propagates through a birefringent medium. To specify the polarization, the state and degree or polarization must be specified. The effect of propagation through a birefringent medium is to change the state of polarization but not the degree of polarization.

The general state of polarization is elliptic, and there are two familiar limiting cases, namely linear and circular. These states are shown in Fig. 6. The figures are produced by the tip of the electric field vector as it moves in a plane perpendicular to the propagation direction. A complete description of the state of polarization includes ellipticity, the orientation with respect to some coordinate system, and the direction (clockwise or counterclockwise) in which the electric field vector rotates.

The degree of polarization is a statistical description of how the state of polarization evolves in time. If the degree of polarization is unity, then the state of polarization is constant in time. If the degree of polarization is zero, then the state of polarization changes randomly in time through all possible states.

Single pass, fiber optic gyroscopes measure rotation rate by measuring the optical intensity of the recombined counter-propagating light waves. This intensity is a function of the phase shift between the counter-propagating light waves. Ideally, this phase shift equals the Sagnac phase shift which is proportional to the rotation rate. The birefringence of the optical fiber can introduce additional phase shifts which may be indistinguishable from the rotation induced phase shift. These birefringence dependent phase shifts are not constant because of the extreme environmental sensitivity of the fiber birefringence.

If polarization selective components exist in the fiber gyroscope, then a change in the optical intensity results from a change in the polarization state due to fiber birefringence. This birefringence dependent intensity change may be indistinguishable from a rotation induced intensity change.

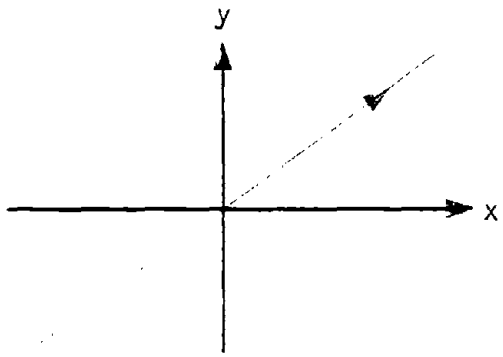

(a) LINEAR

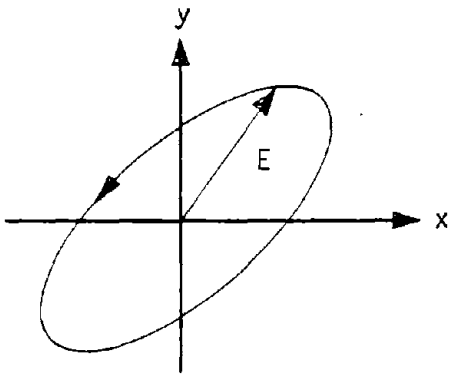

(b) ELLIPTICAL

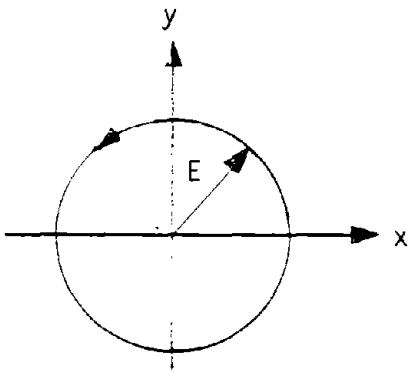

(c) CIRCULAR

Fig. 6--Electric field trajectories in a plane normal to propagation direction for various states of polarization.

The net result of these birefringence dependent phase and intensity changes can be large errors in the measurement of rotation rates. These birefringence dependent changes must be eliminated or reduced in practical fiber gyroscopes, and this requires an understanding of the interaction of polarization and fiber birefringence in these devices.

2. Theoretical Development

A mathematical formalism has been developed which allows calculation of the response of a single pass, fiber gyroscope for any input polarization and any fiber birefringence. This formalism is both a generalization and refinement of an approach reported by Ulrich and Johnson[5] which was limited to input polarizations whose degree of polarization is unity, i.e., where the state of polarization is constant in time.

The state of polarization will be described in terms of basic states. The basic states are chosen as the x and y linear polarization states. Any polarization state can be expressed as a weighted sum of these base states. The degree of polarization is described by the correlation of the coefficients of these base states.

The coherence matrix formalism is chosen to represent the degree and state of polarization. The coherence matrix J is defined in terms of the coefficients of the base states as

$$J = \begin{pmatrix} \langle a_x(t)\ a_x^*(t)\rangle & \langle a_x(t)\ a_y^*(t)\rangle \\ \langle a_y(t)\ a_x^*(t)\rangle & \langle a_y(t)\ a_y^*(t)\rangle \end{pmatrix} \tag{4}$$

where $a_x(t)$ and $a_y(t)$ are the instantaneous values of coefficients of the x and y linear polarization base states, the asterisk denotes the

complex conjugate and the brackets denote the infinite time average. Further details of the coherence matrix and its properties are given in Appendix B.

The optical fiber is modeled as a general, four port linear system. The model for this is shown in Fig. 1 of Appendix A. The four ports are the x and y linear polarization base states at either end of the fiber. Also seen in the figure are the four channels which connect the four ports as shown. The channel is an abstract pathway along which light propagates. This model of the fiber can be described by two Jones matrices, one for propagation in each direction. Ulrich gave the general form for these Jones matrices T in the presence of rotation, which are given as Eqs. 2 and 3 of Appendix A.

Explicit forms for the elements $t(k\ell)$ have been derived. This derivation is treated in Appendix C. The Jones matrices describing the fiber can be rewritten as

$$T_{21} = e^{+j\phi_s/2}\, e^{j\Phi} \begin{pmatrix} \cos\theta e^{j\xi/2} & \sin\theta e^{-j\phi/2} \\ -\sin\theta e^{j\phi/2} & \cos\theta e^{-j\xi/2} \end{pmatrix} \tag{5a}$$

$$T_{12} = e^{-j\phi_s/2}\, e^{j\Phi} \begin{pmatrix} \cos\theta e^{j\xi/2} & -\sin\theta e^{j\phi/2} \\ \sin\theta e^{-j\phi/2} & \cos\theta e^{-j\xi/2} \end{pmatrix} \tag{5b}$$

In these matrices, ϕ_s is the Sagnac phase shift, ϕ is the average phase shift along the fiber, θ is the state-of-polarization rotation parameter (i.e., the state of polarization is rotated by θ), ξ is the linear birefringence of the fiber, and ϕ is a reciprocal birefringence dependent phase

[6]Note that in Appendix C, notation is S_{12}, S_{21} instead of T_{12}, T_{21}.

shift, which can be indistinguishable from the Sagnac phase shift in certain cases. The parameters $\bar{\emptyset}$, θ , ξ , and $\emptyset$ depend on the birefringence in the fiber and are environmentally sensitive. These parameters are defined more completely in Appendix C.

A fiber gyroscope typically contains many components. These components include beam splitting and combining elements, polarizers, polarization controllers, phase shifters and phase modulators. Each component is represented by one or more Jones matrices. The Jones matrix of a fiber gyroscope can be written in terms of the Jones matrices of the components, using matrix multiplication and addition. Let M denote the Jones matrix of the fiber gyroscope. The coherence matrix of the output light J_{out} is related to the coherence matrix of the input as

$$J_{out} = M J_{in} M^{+} \tag{6}$$

where M^{+} is the hermitian adjoint of M . The output intensity can be computed from the output coherence matrix.

3. Unpolarized Operation

This mathematical formalism was applied to a single pass, cw fiber optic gyroscope operated with unpolarized input light. The coherence matrix for unpolarized light of unit intensity is

$$J_{unpolarized} = \begin{pmatrix} 1/2 & 0 \\ 0 & 1/2 \end{pmatrix} \tag{7}$$

This says that unpolarized light has equal average power in the two orthogonal base states and that the coefficients of the base states are uncorrelated, which means that the electric fields in the two orthogonal base states are incoherent and that they cannot form an interference pattern.

The calculated output intensity for unit input intensity for the unpolarized gyroscope in Fig. 7 is

$$I = 1/2 + 1/2\ (\cos^2\theta - \sin^2\theta \cos\phi)\cos\phi_s \qquad (8)$$

where θ describes the rotation of the state of polarization by the fiber, and ϕ is the reciprocal birefringent dependent phase shift. These quantities are derived in Appendix C. In obtaining Eq. (8), the beam splitting/combining elements are assumed ideal. This means that they are lossless, polarization insensitive, and have a 50-50 splitting ratio.

A plot of I versus ϕ_s (Sagnac phase shift) for Eq. (8) is shown in Fig. 8. The curves in Fig. 8 are described by different values of θ and ϕ which are functions of the fiber birefringence. Three features of these curves are of interest. First, the maxima and minima of the curves always occur at the same value of ϕ_s. No translation of the curves along the ϕ_s axis exists for changing values of θ and ϕ. If this type of translation was present, then the Sagnac phase shift would be indistinguishable from ϕ, the reciprocal birefringence dependent phase shifts. Second, the average value of the intensity for these curves is constant. The maxima and minima of the curves expand or contract about the average value with varying birefringence. In conventional, polarized, single pass fiber optic gyroscopes the value of the minima is fixed, while the value of the maxima of the curves changes with varying birefringence. Third, all the response curves in Fig. 8 intercept each other at a family of points which are characterized by the Sagnac phase shift being an odd multiple of $\pi/2$ radians. These points of intersection

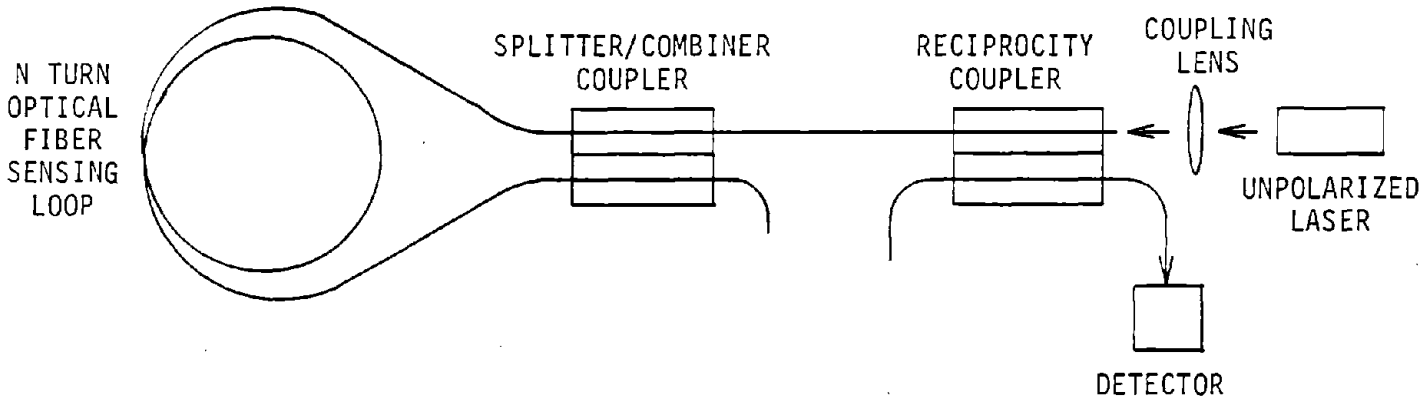

Fig. 7--Schematic of a basic, reciprocal, unpolarized fiber gyroscope.

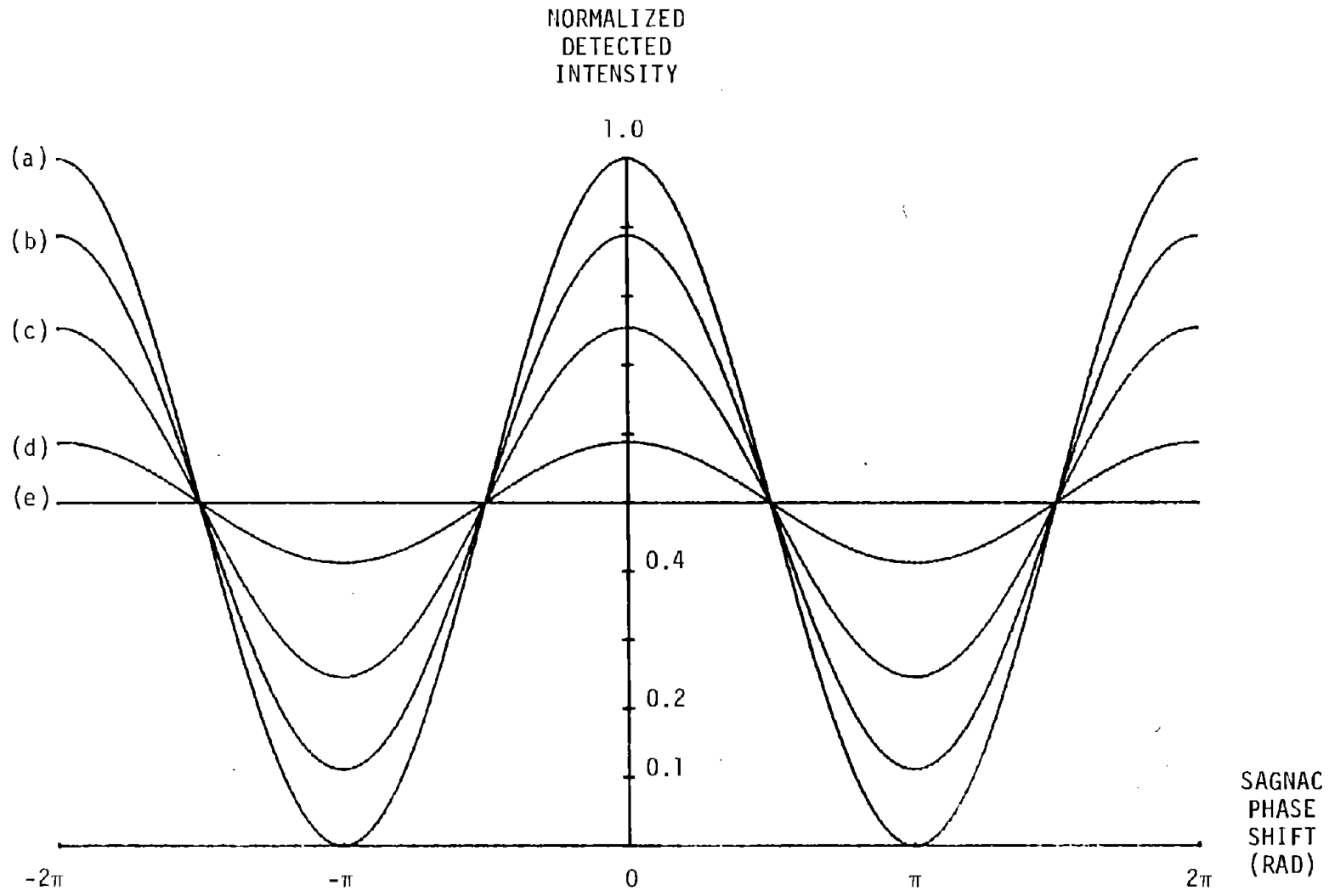

Fig. 8--Normalized output intensity versus Sagnac phase shift for reciprocal, unpolarized gyroscope. The curves are described by the birefringent parameters (θ,ø). (a) (45,0), (b) (20,25), (c) (30,15), (d) (40,5), (e) (45,0).

of the response curves are called stable operating points. If the gyroscope is operating at one of these points, the detected intensity is independent of changing birefringence. The gyroscope is stable with respect to reciprocal changes in the fiber birefringence at these points. An unpolarized gyroscope has been built and operated during the reporting period. It confirmed the theoretical predictions above.

Further calculated cases, and a description of the experimental results, are given in Appendix C.

Advantages of unpolarized fiber optic gyroscopes over conventional polarized fiber optic gyroscopes are expected to be a reduced part count (no polarizer is required), reduced environmental sensitivity, and a reduction in coherent backscattered noise due to the use of two spatially incoherent modes (i.e., the two orthogonal polarization modes).

C. PROPOSED UNPOLARIZED GYROSCOPE

The design shown in Fig. 9 is proposed for an unpolarized gyroscope. It takes full advantage of the operating characteristics described above for unpolarized gyroscopes, to provide a stable output which is linear in the rotation rate over a broad range.

The gyroscope is designed so that the operating point (i.e., values of output intensity and phase shift between the counterpropagating waves) remains at or near one of the stable operating points. This is accomplished by sensing the difference between the output intensity and the average intensity, and using feedback applied to the variable nonreciprocal phase shifter in the sensing loop to cause the output intensity to equal the average intensity. The amount of feedback applied is a measure of the rotation, and is linear in the rotation rate.

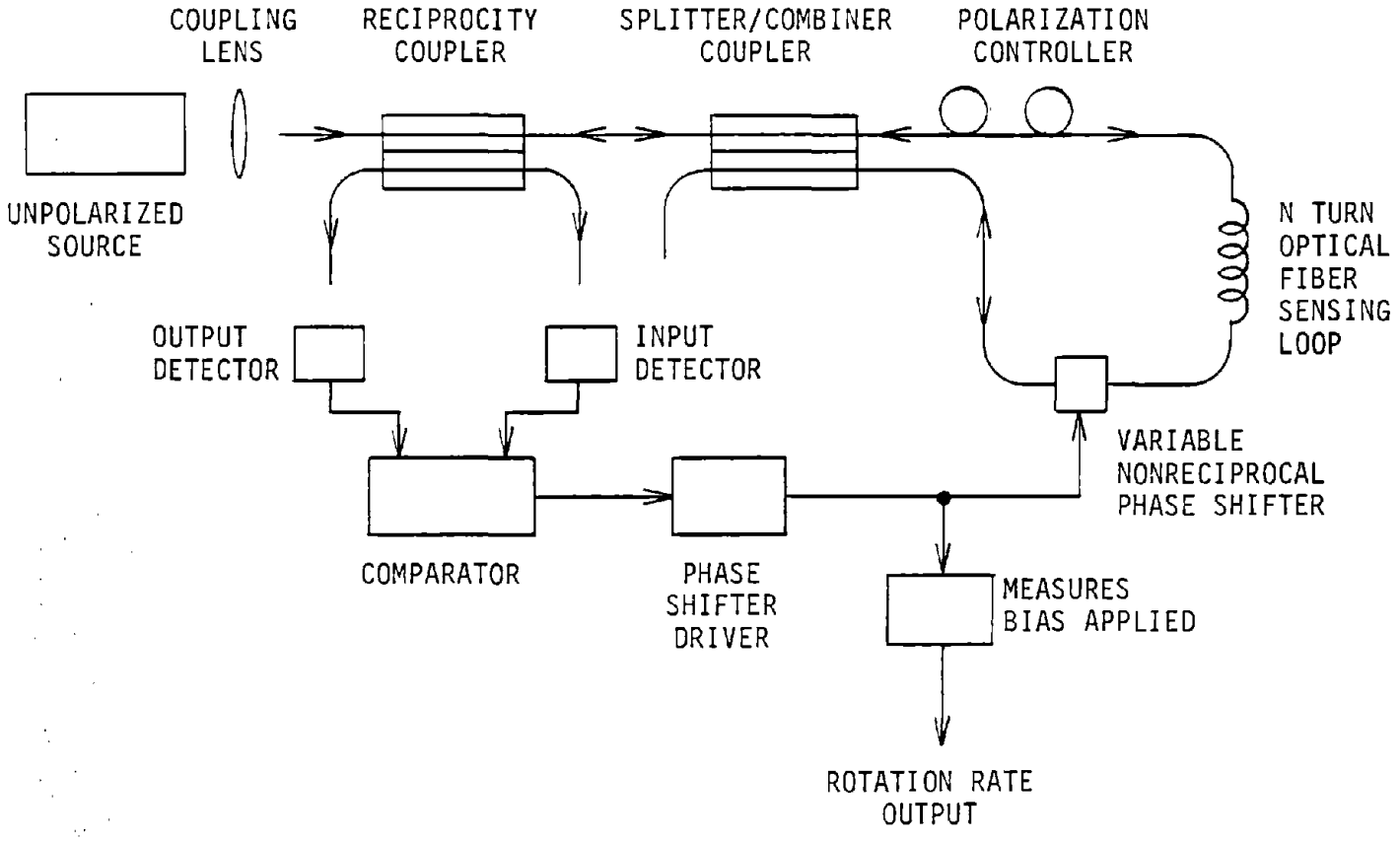

Fig. 9--Schematic of proposed unpolarized fiber gyroscope.

At rest a $\pi/2$ radian phase shift exists between the counterpropagating waves due to the nonreciprocal phase shifter. This nonreciprocal phase shift ϕ_{nr} is additive to the Sagnac phase shift (i.e., $\phi_s \rightarrow \phi_s + \phi_{nr}$). This biases the gyroscope to the first stable operating point. Eq. (8) becomes

$$I = 1/2 + 1/2\ (\cos^2\theta - \sin^2\theta \cos\phi) \cos(\pi/2) = 1/2 . \quad (9)$$

The output intensity at rest equals the average intensity. When the gyroscope is rotated, the Sagnac phase shift is no longer zero. Before feedback is applied to the nonreciprocal phase shifter, Eq. (9) becomes

$$I = 1/2 + 1/2\ (\cos^2\theta - \sin^2\theta \cos\phi) \cos(\phi_s + \pi/2) . \quad (10)$$

The output intensity now differs from the average intensity. Feedback is applied to the nonreciprocal phase shifter so that the output intensity above equals the average intensity. Eq. (10) becomes

$$I = 1/2 + 1/2\ (\cos^2\theta - \sin^2\theta \cos\phi) \cos(\phi_s + \pi/2 + \phi_{nr}) = 1/2 . \quad (11)$$

The nonreciprocal phase shift which accomplishes this is equal to, but opposite in sign from, the Sagnac phase shift. If the nonreciprocal phase shifter is a Faraday cell, then the drive current is proportional to the nonreciprocal phase shift and hence the Sagnac phase at the stable operating point. By measuring the drive current the rotation rate is obtained and the drive current is also linear in the rotation rate.

The unpolarized gyroscope depicted in Fig. 9, implements the above scheme. Light from an unpolarized source is coupled into the fiber by a coupling lens. It passes through a reciprocity coupler which is a fiber-

to-fiber evanescent field directional coupler. Approximately half of the light is sent to the input detector. The resulting signal is used to compute the average output intensity. This is done to compensate for laser power and input coupling fluctuations.

The remaining light propagates to the splitter/combiner coupler where it is split into two waves of approximately equal power, which then propagate in opposite directions around the N-turn, optical fiber sensing loop. The variable nonreciprocal phase shifter introduces a phase shift between the counterpropagating waves in addition to any rotation induced phase shift. A polarization controller is provided to reduce any errors introduced by a residual degree of polarization of the light source. It also exerts control over the slope (i.e., $dI_{out}/d\emptyset_s$) of the output intensity at the stable operating point.

The light waves are recombined by the splitter/combiner coupler and propagate to the reciprocity coupler, where half of the power is then sent to the output detector. The electrical signal from this detector goes to a comparator where it is compared with the average intensity which has been computed from the electrical signal of the input detector. A difference in these signals causes the phase shifter driver to vary the nonreciprocal phase shift in the sensing loop until the output and average intensities are equal. The gyroscope is thus maintained at the stable operating point.

The signal which the driver applies to the variable non-reciprocal phase shifter is measured and the rotation rate is computed. Since the gyroscope is at or near a stable operating point, it is relatively insensitive to reciprocal birefringent changes in the sensing loop.

The polarization controller controls the slope $(dI_{out}/d\emptyset_s)$ of the response curve to keep it from going to zero (environmental fading). The control is exerted over the birefringent parameters θ and $\emptyset$ in Eq. (8). The degree of control required is quite loose since the slope does not need to be held constant at a particular value, but just needs to be kept away from zero. The polarization control also relaxes the limit on the residual degree of polarization of the source. If the source is not completely unpolarized, then a phase measurement error appears which is proportional to the degree of polarization. This phase measurement error is reduced significantly by the polarization controller.

All components except for the variable nonreciprocal phase shifter are on hand. The phase shifter still needs development, before it can be used in the proposed unpolarized gyroscope.

Advantages of this unpolarized gyroscope are reduced noise due to coherent backscattering and reciprocal birefringence changes, linear output over a broad dynamic range, a reduced requirement on degree of polarization control, and omission of the high quality polarizer needed for polarized gyros.

D. NOISE REDUCTION

At the beginning of the present reporting period all known fiber rotation sensors appeared to be limited in their minimum measurable rotation rate, to values much higher than the theoretical limit due to quantum noise. During the reporting period we studied this problem intensively and came to the conclusion that this was largely due to coherent Rayleigh backscattering of the primary circulating waves. This is scattering from the material

inhomogeneities in the fiber. Such inhomogeneities are characteristic of all fibers now fabricated, and this phenomena is responsible for the principal optical propagation loss in fibers. However, some portion of the light is scattered into a direction so that it is still confined to the core and propagates along the fiber in the opposite direction to the original signal. This occurs in all fibers. In the ring Sagnac sensor this backward scattered signal from each wave, of course, propagates along with the injected opposite traveling wave, is guided to the detector where it contributes to the overall noise and thus degrades the signal-to-noise-ratio. The primary limitation to rotation sensitivity, however, is the phase error produced by this coherent backscattering. To the extent that the backscattered waves are coherent with the primary signal waves they add vectorially at unpredictable phases that are not identical for the two oppositely directed waves. The resulting measured phase shift is indistinguishable from that caused by rotation. A detailed analysis of this scattering and its effect is given in Appendix D which is the text of a published paper describing our work on this problem done under this contract.

We have been considering various methods for overcoming this problem and describe them briefly below. Further details on these proposed methods will also be found in Appendix D.

The phase error we have described above can be minimized by reducing the coherence between primary and backscattered waves. One method of randomization is by phase modulation of the loop.[6-8] If the phase modulation

---

[6]K. Böhm, P. Russer, E. Weidel, and R. Ulrich, Optics Letters 6, 64 (1981).

[7]R. A. Bergh, H. C. Lefevre, and H. J. Shaw, Optics Letters 6, 198 (1981).

[8]R. A. Bergh, H. C. Lefevre, and H. J. Shaw, IOOC '81 Technical Digest, p. 116 (1981).

is rapid enough to allow sampling of the signal at a frequency M, the cumulative rotation error is reduced in proportion to $M^{-1/2}$.

A greater reduction in coherence can be achieved by using a source having a short coherence length (e.g., a laser diode).[9,10] In this case only those scatterers located such that the round trip transit time from the input differs from the loop transit time by less than the coherence time of the source will make large contributions to the phase error. This means that most of the phase error is due to those scatterers located halfway along the loop within a fiber segment equal in length to the coherence length of the source. Scatterers located in other parts of the fiber contribute to the phase error to a lesser degree, the extent of which is determined by the coherence properties of the source.

These methods have been tried in another program at Stanford and have increased fiber gyro sensitivity by orders of magnitude, but significant error still remains. One way to further reduce this error is to use signal pulses that are short compared to the loop transit time. (Alternatively, one could use longer pulses that are chirped to form the spectral equivalent of the short pulses, thereby avoiding peak power problems.) The output of the loop equal to the pulse length in the fiber contributes to the error.

While the use of short pulses may appear to yield the same error reduction as would the use of a source having an equally short coherence time, pulsed operation in fact has several advantages. The offending segment of the loop is more clearly defined by a signal pulse than by the source coherence time. Furthermore, the self-gating aspect of pulse operation

---

[9] K. Böhm, P. Marten, K. Peterman, and E. Weidel, IOOC '81, Post Deadline Paper TuL7 (1981).

[10] R. A. Bergh, H. C. Lefevre, and H. J. Shaw (submitted for publication).

insures that scatterers located elsewhere in the loop make no contribution to either the phase error or the shot noise. This allows us to concentrate on reducing the backscattering efficiency of only this short segment of fiber as a means of reducing the backscattering error even further (Fig. 10). We propose that this segment of the loop be:

(1) index matched to reduce the capture efficiency of the fiber,

(2) replaced by an ultra-pure fiber segment having few scatterers,

(3) replaced by a hollow light guide, or

(4) evacuated entirely to insure that no sources of scattering or reflection are present.

Finally, our analysis indicates that, all other parameters being constant, the use of a longer signal wavelength reduces the phase error due to backscattering by roughly λ^{-1} (Fig. 11).

It is probably that by implementing these techniques the sensitivity of existing fiber gyros can be substantially improved.

MODIFIED FIBER SEGMENT

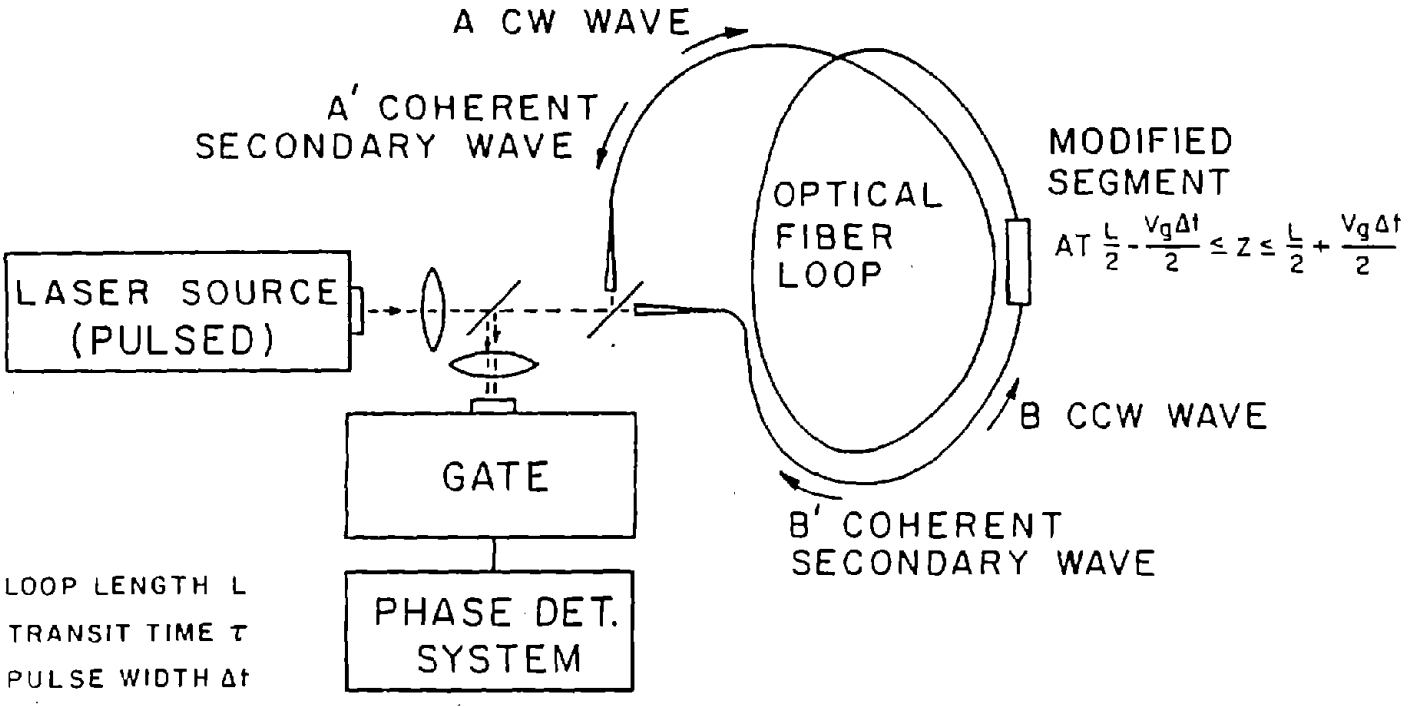

FIGURE 10

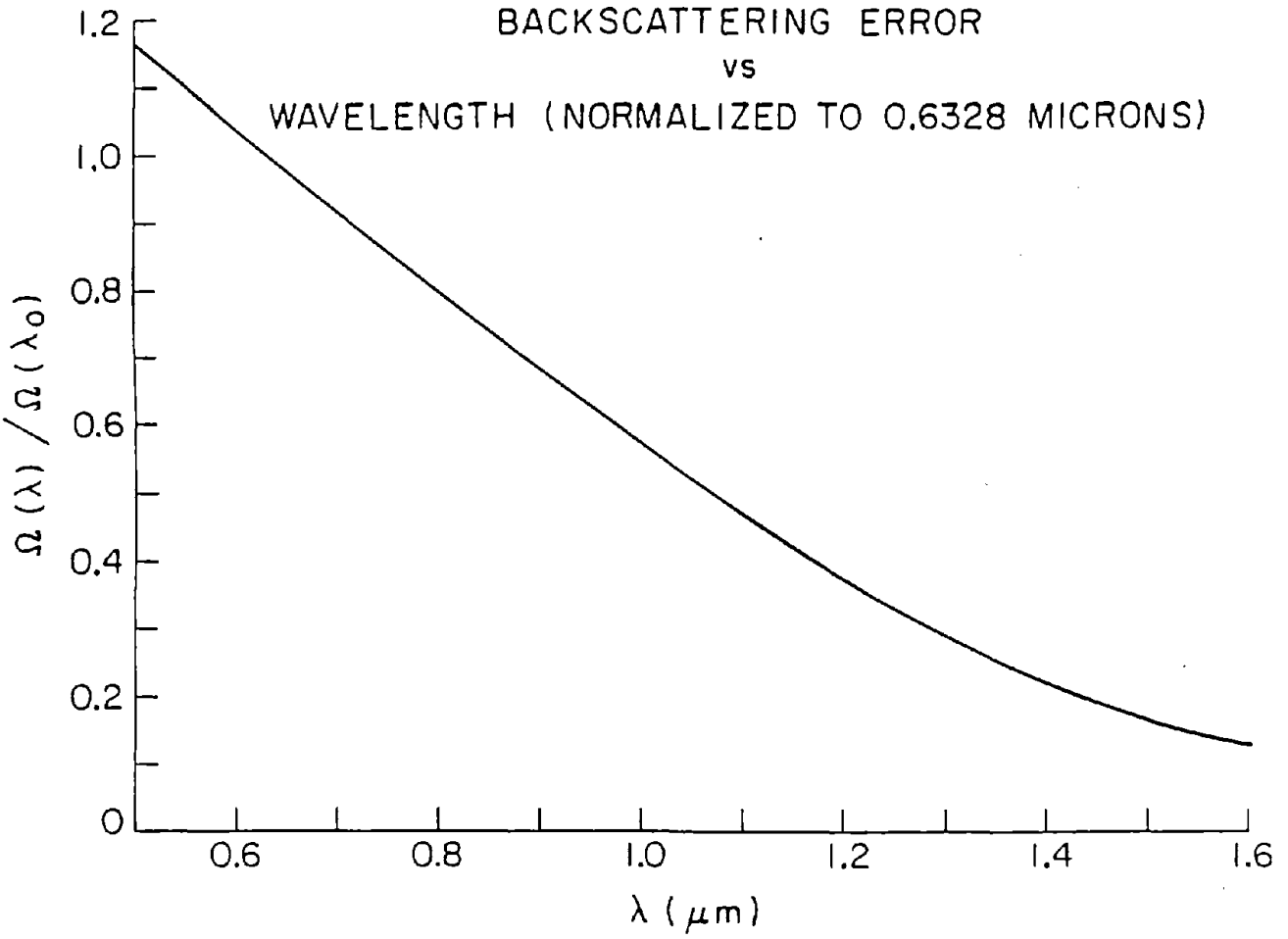
BACKSCATTERING ERROR
vs
WAVELENGTH (NORMALIZED TO 0.6328 MICRONS)
1.2
1.0
0.8
0.6
0.4
0.2
0
Ω (λ) / Ω (λo)
0.6
0.8
1.0
1.2
1.4
1.6
λ (μm)

FIGURE 11

APPENDIX A

STABILITY OF FIBER OPTIC ROTATION SENSORS UNDER VARIOUS POLARIZATION CONDITIONS

by

G. Pavlath and H.J. Shaw

Preprint

G.L. Report No. 3163

August 1980

supported by

F49620-80-C-0040

Edward L. Ginzton Laboratory
W.W. Hansen Laboratories of Physics
Stanford University
Stanford, California

I. INTRODUCTION

Efforts are being made in various laboratories[1-10] to develop fiber optic rotation sensors (FORS) as alternatives to mechanical gyroscopes and ring laser gyros (RLG) in some applications. All FORS's utilize the Sagnac effect[11] in a ring interferometer. The ring interferometer is formed from a length of "single" mode optical fiber wound N times around an area A. In the presence of rotation, countra-directional optical waves propagating around the ring interferometer experience a phase shift (Sagnac Phase shift ϕ_s) given as

$$\phi_s = \frac{8\pi\ NA}{\lambda c}\ \Omega \qquad (1)$$

where λ and c are the free space values of wavelength and speed of light and Ω is the rotational velocity of the ring interferometer. In most FOR's the intensity of the interferometer pattern of the ring interferometer is monitored in a localized area. Changes in the rotation rate of the FORS give rise to change in the Sagnac phase shift which in turn is detected as a change in intensity in the monitored area of the interference pattern.

While the fringe pattern appears relatively stable to the eye, it actually possesses variations with time which are sources of error. Environmental effects other than rotation, such as temperature, vibration, etc., can cause variations in both the positions and intensities of the fringe pattern, which often cannot be distinguished from the desired changes due to rotation. It has been shown[6,12] that by using polarized light at the input to the interferometer, and using polarization filters in the output, the operation of the sensing loop can be made completely reciprocal, and

the positions of the interference fringes are then stable against environmental changes which are homogeneous over the space occupied by the sensing loop. However, the intensity and contrast of the fringes can still be environmentally affected. Work is being done[13,14] on approaches to reducing these effects.

In the following sections we examine further the effects of polarization on the operation of a FORS. This includes theoretical and experimental investigation of operation using polarized, unpolarized, and partially polarized light.

II. THEORY

Real "single" mode fibers propagate two orthogonal polarization modes. These two modes have slightly different propagation velocities. Environmental effects mix the two polarization modes. This mixing of the orthogonal modes can result in the instabilities observed in FORS's if proper care is not taken. It is important for the theoretical analysis to realize that while the state of polarization can change in a real "single" mode fiber, the degree of polarization is unchanged. This allows us to treat the fiber as a four port linear system. In Fig. 1, the four ports are shown explicitly. Although the polarization states are labelled x and y they can, in general, be any two orthogonal polarization states. Also shown schematically in Fig. 1 are the possible channels between the four ports. A channel is characterized by a complex scattering coefficient. The matrices describing the scattering between the fiber ends among the polarization modes are recognized as Jones matrices for a birefringent element. This representation

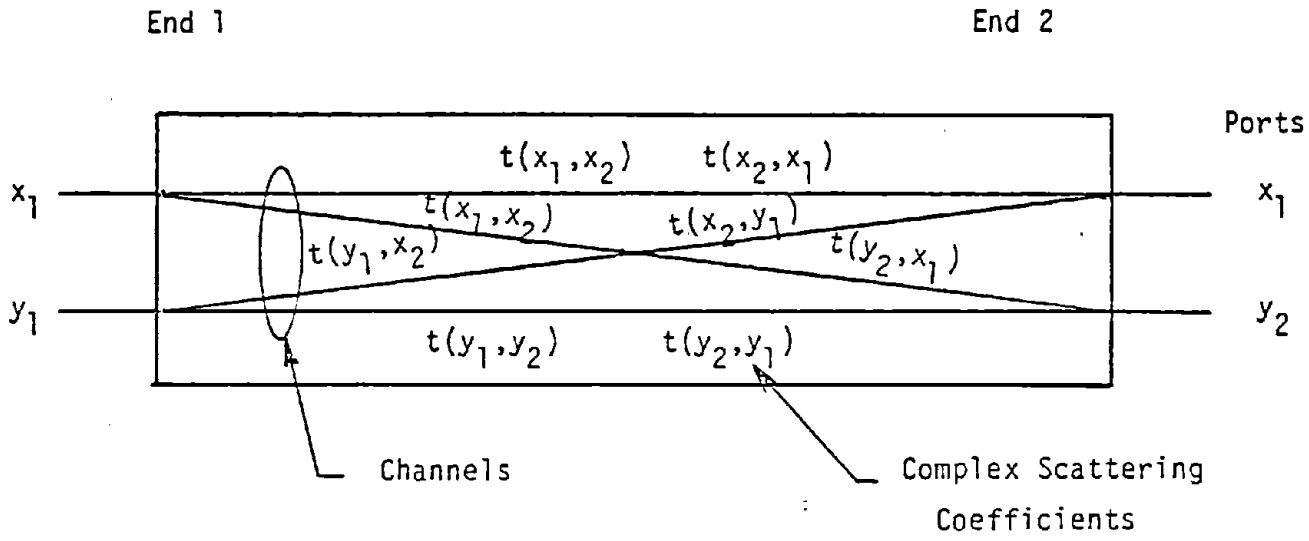

Fig. 1--Four-port linear system model of a single mode fiber. The ports are x_1, x_2, y_1, y_2. The channels between the ports are shown schematically along with their complex scattering coefficients.

of a real "single" mode fiber by Jones matrices was first presented by Ulrich, et al.[12]

In Fig. 2, the system which we will analyze is shown. We have a length of single mode fiber wound N times around an area A. We represent the beam splitting and recombining elements as a black box. We will neglect the details of the beam splitting and recombining in our calculations. We should point out, however, that these details can, in principle, be a source of nonreciprocity in the system unless properly configured. Inclusion of these details can give rise to scale factor changes, a phase shift, reduction in contrast, and a change in the degree of polarization. We are interested here only in the effects of the fiberoptic sensing loop on the system. We assume that the laser can be operated with any degree of polarization required. In Fig. 2 a general polarization analyzer can be inserted before the detector to pass a given polarization state only.

The Jones matrix for propagation from end 1 to end 2 (Fig. 1) is T_{21}, and for propagation from end 2 to end 1 is T_{12}. This Jones formalism allows the inclusion of the birefringent effects which are in general present in real single mode fibers. The matrices T_{21} and T_{12} are unitary for zero rotation rate. With rotation present the explicit forms for T_{21} and T_{12} are

$$T_{21} = e^{j\phi_s/2} \begin{bmatrix} t(x_2,x_1) & t(x_2,y_1) \\ t(y_2,x_1) & t(y_2,y_1) \end{bmatrix} \tag{2}$$

$$T_{12} = e^{-j\phi_s/2} \begin{bmatrix} t(x_1,x_2) & t(x_1,y_2) \\ t(y_1,x_2) & t(y_1,y_2) \end{bmatrix} \tag{3}$$

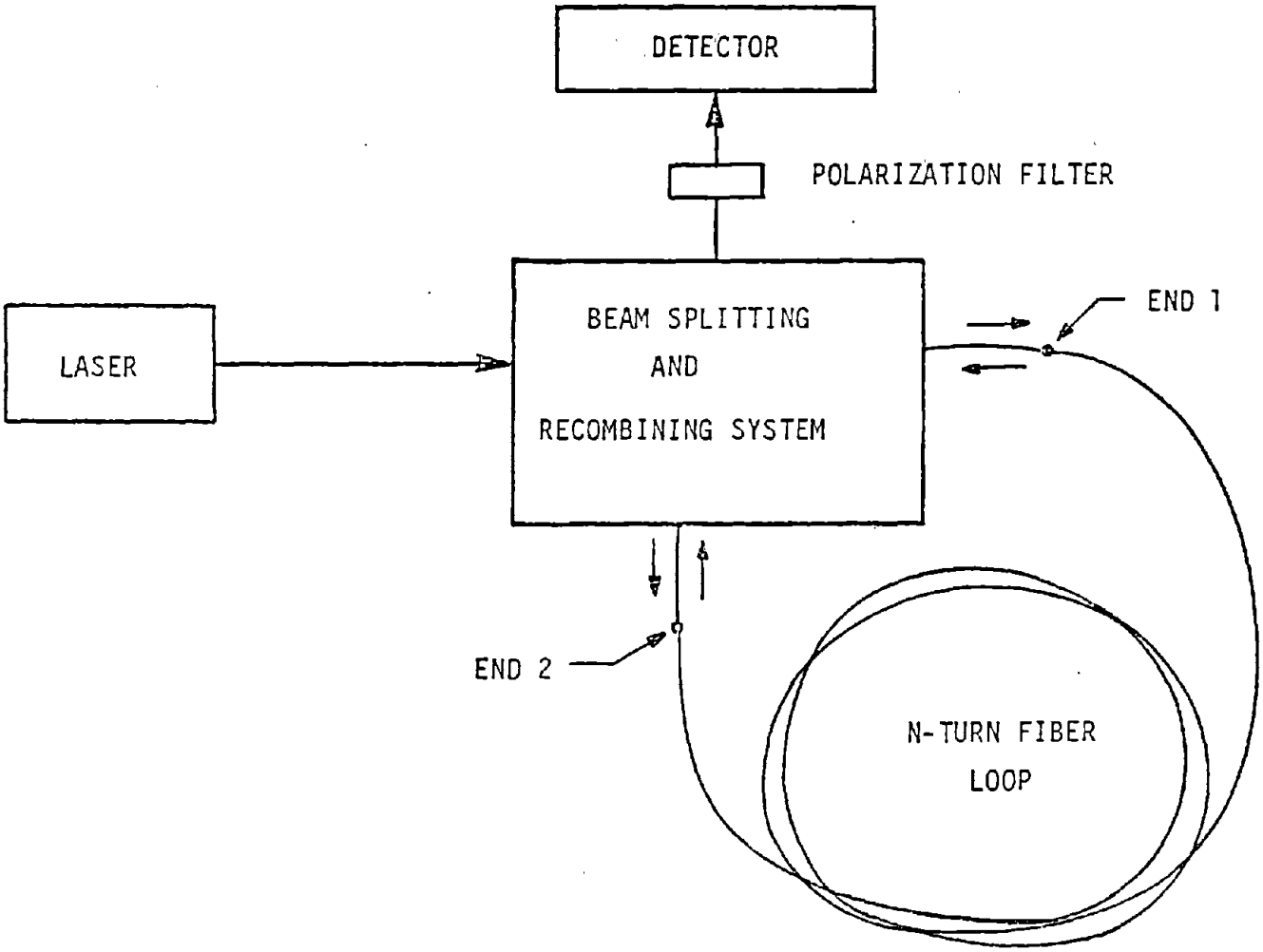

Fig. 2--Schematic of system analyzed.

Here ϕ_s is the Sagnac phase shift as given by Eq. (1). The t's (Fig. 1) are the complex scattering coefficients of the fiber, and are environmentally dependent. The principle of reciprocity imposes the following condition

$$t(k,\ell) = t(\ell,k) \tag{4}$$

This means that the effect of a channel is independent of the direction in which the channel is traversed. Equation (4) is valid only if there is no rapidly changing gradient along the fiber. By rapid we mean fast compared to the transit time of the fiber. In our calculations, we will assume that the fiber is lossless and that the optical power propagating in each direction in the fiber are equal.

The input into each end of the fiber is represented as a vector $\vec{E}_{in}$, where the components of the vector are the $\vec{E}$ fields of the two polarization modes. Allowing the input to propagate around the fiber in opposite directions and recombining the outputs from each end of the fiber, we obtain

$$\vec{E}_{out} = T_{21}\,\vec{E}_{in} + T_{12}\,\vec{E}_{in} \tag{5}$$

This signal can be passed through a general polarization analyzer represented by a matrix P. The detected E field is then

$$\vec{E}_{det} = P\,\vec{E}_{out} \quad . \tag{6}$$

We will now calculate $\pm$ det $= |\vec{E}_{det}|^2$ for various $\vec{E}_{in}$ and polarization analyzers.

III. CALCULATED CASES

Case 1. We will let $\vec{E}_{in}$ be polarized in the first state of polarization. The polarization analyzer will pass this state. The forms for $\vec{E}_{in}$ and P are

$$E_{in} = \{1,0\} \tag{7}$$

$$P = \begin{bmatrix} 1 & 0 \\ 0 & 0 \end{bmatrix} \tag{8}$$

We now perform the operation in Eqs. (5) and (6) and calculate the normalized detected intensity I_{det}.

$$I_{det} = 1/2\left|t(x_2,x_1)\right|^2(1 + \cos \phi_s) \tag{9}$$

Figure 3 shows a plot of I_{det} versus ϕ_s for various environmental conditions, i.e., values of $t(x_2,x_1)$. The environment conditions are parameterized by θ and ϕ. θ is a measure of the power transfer between the two polarization modes. ϕ is also the non-reciptocal phase shift between the contradirectional waves which enter the fiber in one polarization and exit the fiber in the other polarization. Refer to Appendix A for the derivation θ and ϕ as environmental parameters. The plots are sinusoidal. The minimum values of the plots (i.e., $I_{det} = 0$) are insensitive to environmental changes. Unfortunately the sensitivity to rotation at the minima is also zero. The maxima of the plots are environmentally sensitive. The value of the maximum varies between 0 and 1. The position (i.e., the value of ϕ_s for which I_{det} is maximum) is not environmentally dependent. This means that various detection schemes (i.e., detection in quadrature) can be used to compensate for the environmentally produced intensity changes.

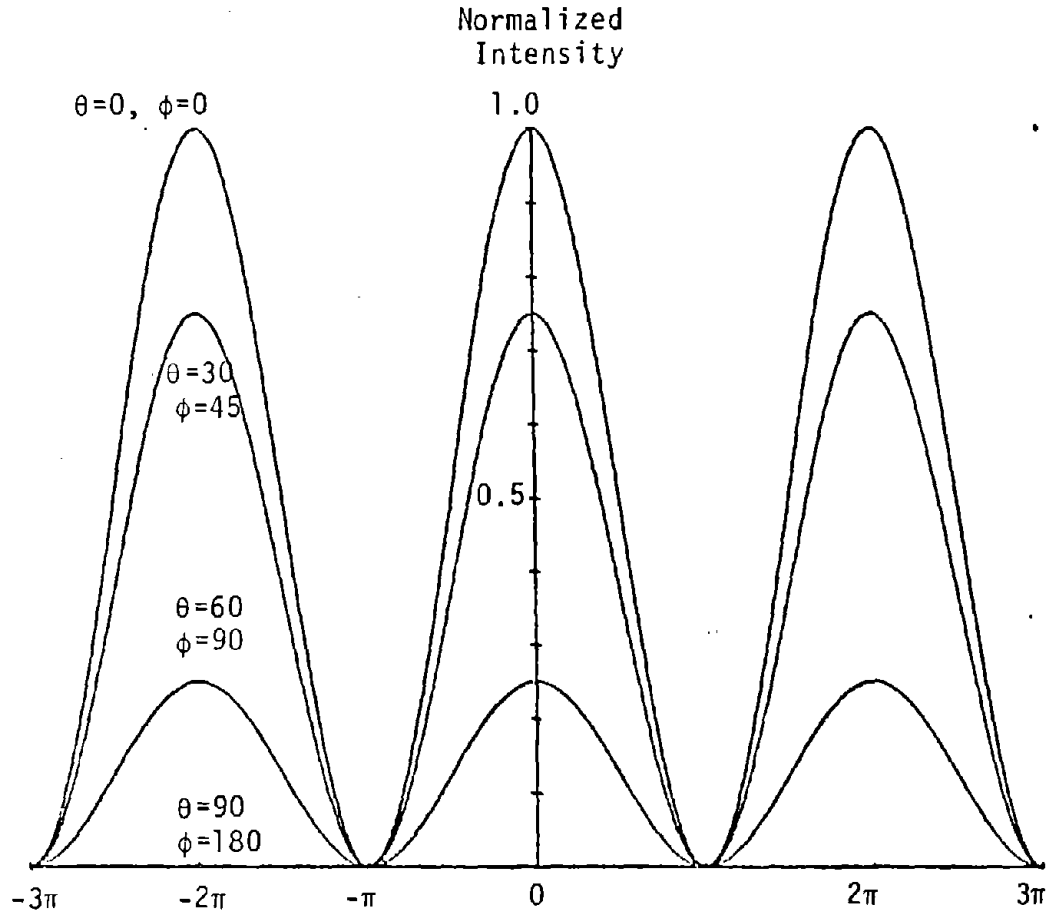

Fig. 3--Normalized intensity vs Sagnac phase shift for polarized input. Analyzer set to pass input polarization. Parameter θ and ϕ are discussed in the text below Eq. (9).

These schemes give large errors when $t(x_1,x_2) \to 0$. To prevent this polarization conserving fiber or a means of active polarization control in the fiber is necessary.

Case 2. We will let $\vec{E}_{in}$ be defined as in Case 1, but the polarization analyzer will now pass the orthogonal polarization state. The form for P is now

$$P = \begin{bmatrix} 0 & 0 \\ 0 & 1 \end{bmatrix} \tag{10}$$

Using Eqs. (7) and (10) in Eqs. (5) and (6) we obtain the normalized detected intensity

$$I_{det} = 1/4|t(y_2,x_1)|^2 + 1/4|t(y_1,x_2)|^2 + 1/2|t(y_2,x_1)||t(y_1,x_2)| \times \cos\{\phi_s + \arg[t(y_2,x_1)] - \arg[t(x_1,x_2)]\} \tag{11}$$

Figure 4 shows plots of I_{det} versus ϕ_s for the same environmental conditions as was used for Fig. 3. All plots in this paper will use the same set of environmental conditions. See Appendix A for the analytical form of the T's used in the calculations. The plots are again sinusoidal. The position of the minima and maxima are now environmentally sensitive. The value of the minima is still environmentally insensitive. The value of the maximum is environmentally sensitive. Because the positions of the minima and maxima can change, there is no detection scheme which will allow one to measure ϕ_s . This case is an incorrect mode of operation of a FORS.

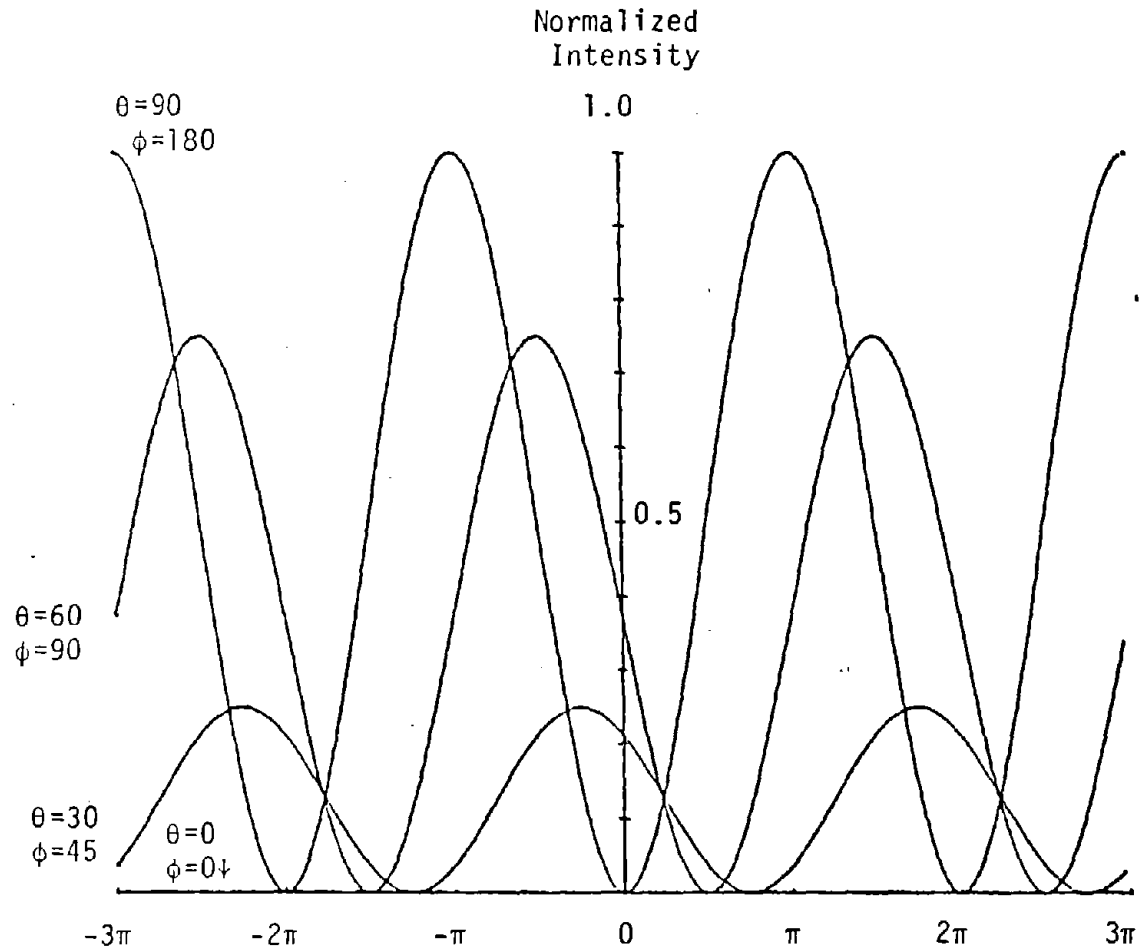

Fig. 4--Same as Fig. 3, except that analyzer is set to reject input polarization.

Case 3. $\vec{E}_{in}$ is the same as in the two previous cases. There is no polarization analyzer before the detector. In this case the normalized detected intensity is computed to be

$$I_{det} = 1/2|t(x_2,x_1)|^2(1 + \cos\phi_s) + 1/4|t(x_2,x_1)|^2 + 1/4|t(y_1,x_2)|^2 + 1/2|t(y_2,x_1)||t(y_1,x_2)|\cos\{\phi_s + \arg[t(y_2,x_1)] - \arg[t(y_1,x_2)]\} \quad (12)$$

Figure 5 shows plots of I_{det} versus ϕ_s for the same set of environmental conditions as before. The positions of the minima and maxima vary with the environment. This case is also an incorrect mode of operation of a FORS. It is interesting to note that in Fig. 5 the average value or "DC" level of the plots are constant at a value of 1/2. The minima of the plots are now environmentally sensitive.

Case 4. We will now treat the case where the input light is completely unpolarized. We will represent the input vector as

$$\vec{E}_{in} = E_x(t)e^{j\phi(t)/2} , E_y(t)e^{-j\phi(t)/2} \quad (13)$$

ϕ is a random variable uniformly distributed over the interval $(-\pi,\pi)$. $E_x(t)$ and $E_y(t)$ are the instantaneous fields of the two polarization components. The time averaged values of the squared magnitudes of $E_x(t)$ and $E_y(t)$ are

$$\overline{|E_x(t)|^2} = \overline{|E_y(t)|^2} = I/2 \quad (14)$$

where I is the total intensity of the light. There is no polarization analyzer before the detector. Substituting Eq. (12) into Eq. (5), finding

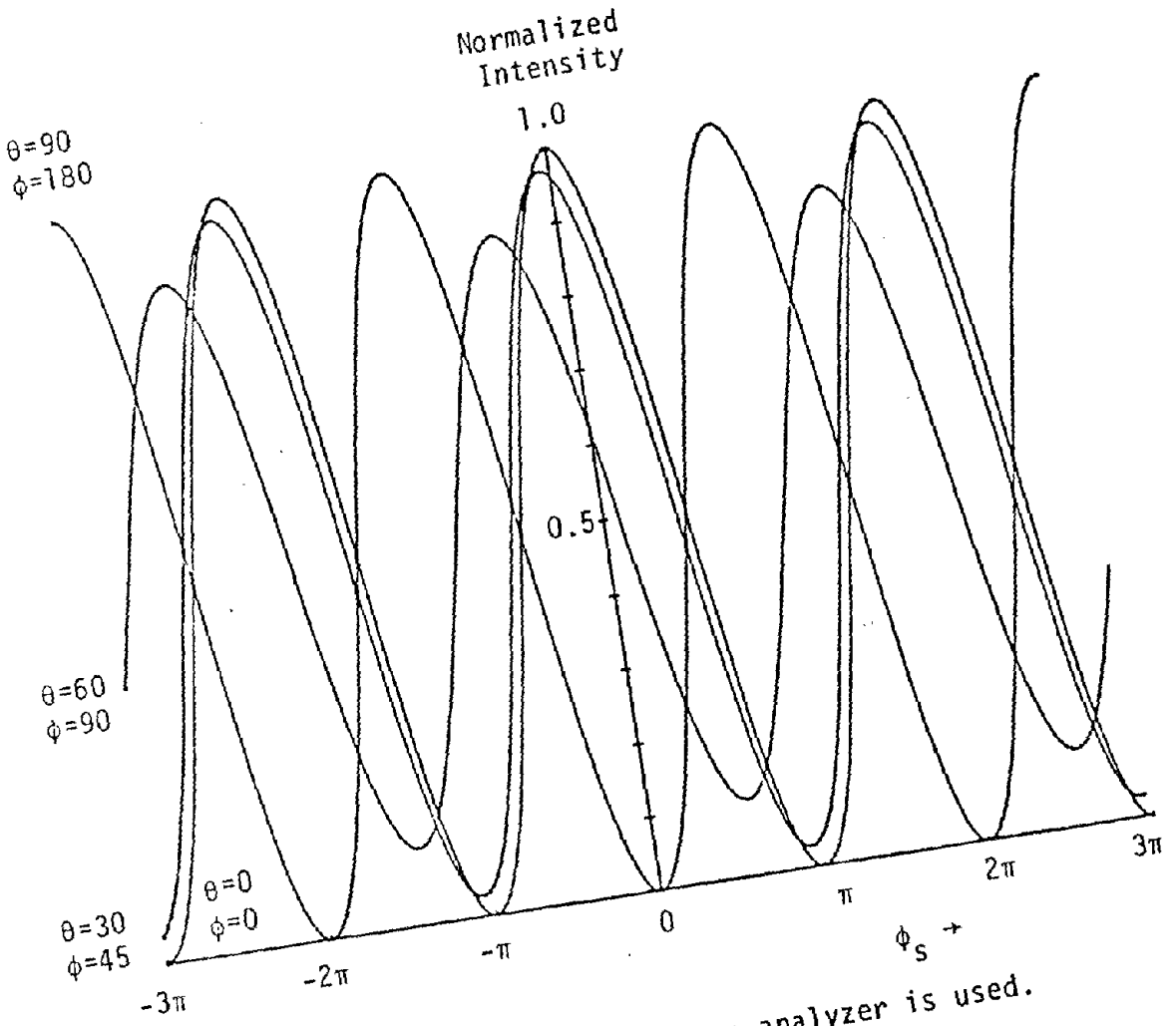

Fig. 5--Same as Fig. 3 except no analyzer is used.

the magnitude squared of $\vec{E}_{det}$, taking the time average, and performing some algebraic manipulations we obtain for the normalized, time averaged, detected intensity

$$I_{det} = 1/2 + 1/2(1 - 1/2|t(x_2,y_1) - t(x_1,y_2)|^2)\cos \phi_s \qquad (15)$$

This equation is valid if the coherence time of the polarization of the light source is much shorter than the response time of the detection system used. Figure 6 shows plots of I_{det} versus ϕ_s for the standard set of environmental conditions used before. The position of the minima and maxima are again environmentally insensitive. The average value of the detected intensity is again constant at a value of 1/2 .

The most important point to realize is the behavior of the detected intensity at the $\pi/2$ points (i.e., $\phi_s = m\,\pi/2$, $m = \pm 1, \pm 3, \ldots$). If the FORS is biased to operate at a $\pi/2$ point, there will be no environmental dependence of the detected intensity. The FORS will be stable. The sensitivity or scale factor at the $\pi/2$ point is still environmentally dependent. This environmental dependence can be handled in various ways which are outside the scope of this paper.

In practice it is difficult to obtain sources of completely unpolarized light of sufficient brightness and of such a geometry as to couple efficiently into a single mode optical fiber. This problem can be overcome by using two linearly polarized sources which are uncorrelated. The plane of polarization of the sources are at right angles to each other. Another method is to use a linearly polarized source whose plane of polarization rotates rapidly. A much more serious problem is that the optical elements exterior to the loop are in general polarization sensitive. These elements tend to partially

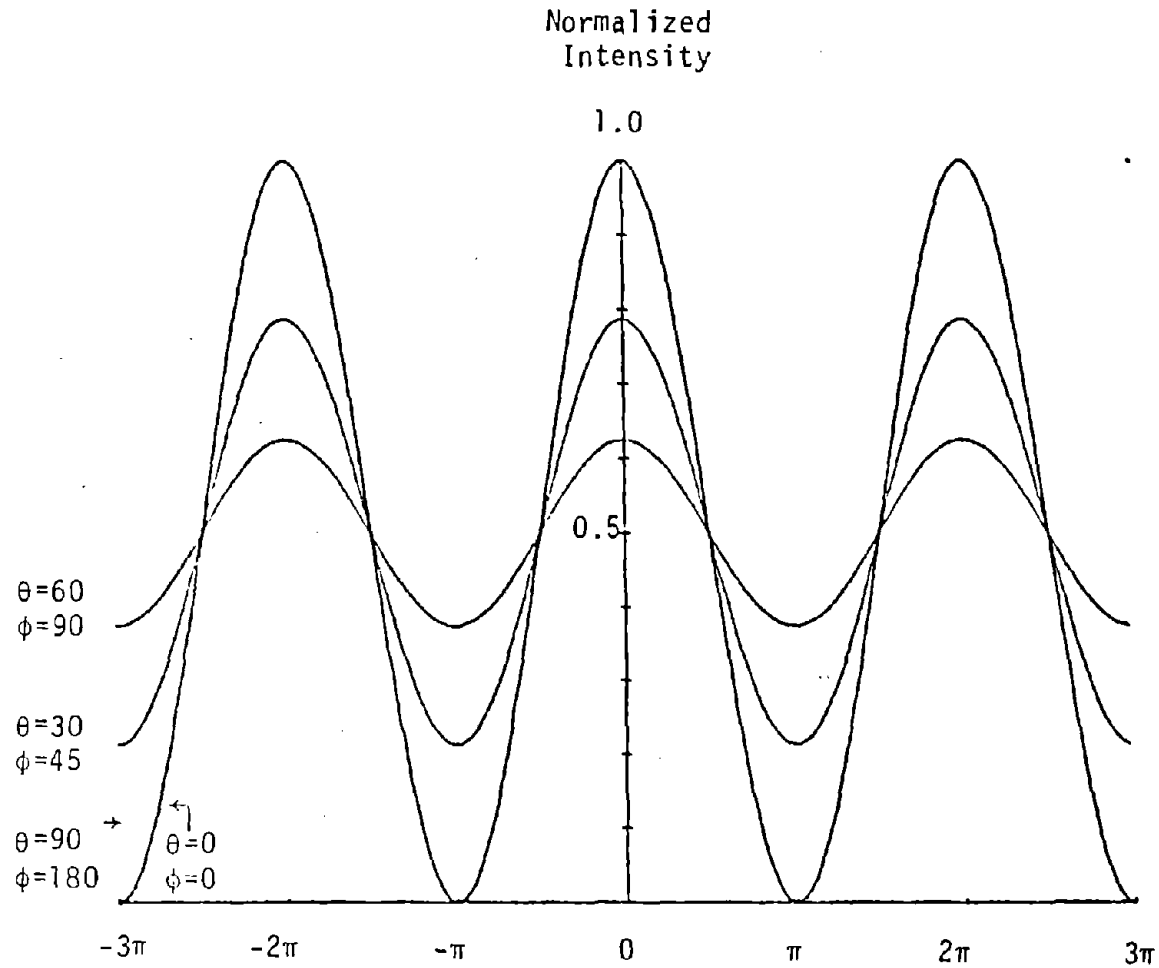

Fig. 6--Same as Fig. 3, except that input is completely unpolarized, and no analyzer is used.

polarize the input light. Because of these two problems in obtaining completely unpolarized light at the input to the fiber optic sensing loop, it is necessary to determine the behavior of the FORS for partially polarized input.

Case 5. Partially polarized input with degree of polarization P. For simplicity we assume that the degree of polarization P of the contra-propagating waves are equal.[15] A wave of degree of polarization P can be decomposed on an intensity basis into a completely polarized wave (P = 1) and a completely unpolarized wave (P = 0). If I_{tot} is the total intensity of the partially polarized wave, then the intensities of the polarized and unpolarized components of the wave are

$$I_{polarized} = P\, I_{tot} \tag{16}$$

$$I_{unpolarized} = (1 - P) I_{tot} \tag{17}$$

The response of the FORS to a partially polarized input can be expressed as the sum of the responses of the FORS to the polarized and unpolarized components of the partially polarized input.

Let there be no analyzer before the detector. The response is obtained by combining Eqs. (11), (15), (16) and (17). The normalized detected intensity can be expressed as

$$\begin{aligned} I_{det} = {} & \frac{P}{2}\, 2\left|t(x_2,x_1)\right|^2 \cos^2 \phi_s/2 + \frac{P}{4}\left|t(y_2,x_1)\right|^2 + \frac{P}{4}\left|t(y_1,x_2)\right|^2 \\ & + \frac{P}{2}\left|t(y_2,x_1)\right|\left|t(y_1,x_2)\right| \cos\left\{\phi_s + \arg[t(y_2,x_1)] - \arg[t(y_1,x_2)]\right. \\ & \left. + \frac{(1-P)}{2}\left[1 + (1 - \left|t(x_2,x_1) - t(x_1,x_2)\right|^2)\cos\phi_s\right]\right\} \end{aligned} \tag{18}$$

Figures 7, 8, and 9 are the plots of I_{det} versus ϕ_s from Eq. (18) for $P = 0.25$, 0.50, and 0.75 respectively. The same environmental conditions are used as before. The average value of the detected intensity is still constant. The position of the maxima and minima are environmentally sensitive. The degree of sensitivity increases as the degree of polarization increases. For partially polarized inputs the $\pi/2$ points are no longer stable. We now ask what maximum degree of polarization is allowable for a given sensitivity to rotation of a FORS, assuming that the environmentally produced phase and amplitude shifts in the sensing loop are the limiting factors. We consider a FORS biased to the $\pi/2$ point. Assuming no noise, and a degree of polarization $P = 0$, we rotate the gyroscope at some angular velocity Ω, and calculate the intensity change $I(\Omega)$. We next let the degree of polarization be nonzero. We then calculate the maximum environmentally produced intensity change I_{max}(Environment) at zero rotation rate $(\Omega = 0)$. We then ask what is the value of the degree of polarization P for which $I(\Omega) = I_{max}$(Environment). This value of P is the maximum value of P allowable for a minimum rotation sensitivity Ω. We assume a fiber optic sensing loop enclosing an area of 1 m^2 with 250 turns and operated at 6328 $\mathring{A}$. We assume a desired sensitivity of 3 deg/hr, which is about an order of magnitude better than has been obtained. This rotation rate corresponds to a Sagnac phase shift, Eq. (1), of 0.3×10^{-3} rad. For these conditions we obtain a maximum degree of polarization of 8×10^{-5}. This is quite small, and may be difficult to obtain in practice. If one is able to control the state of the polarized part of the partially polarized wave in the fiber optic sensing loop, the limit on degree of polarization is reduced.

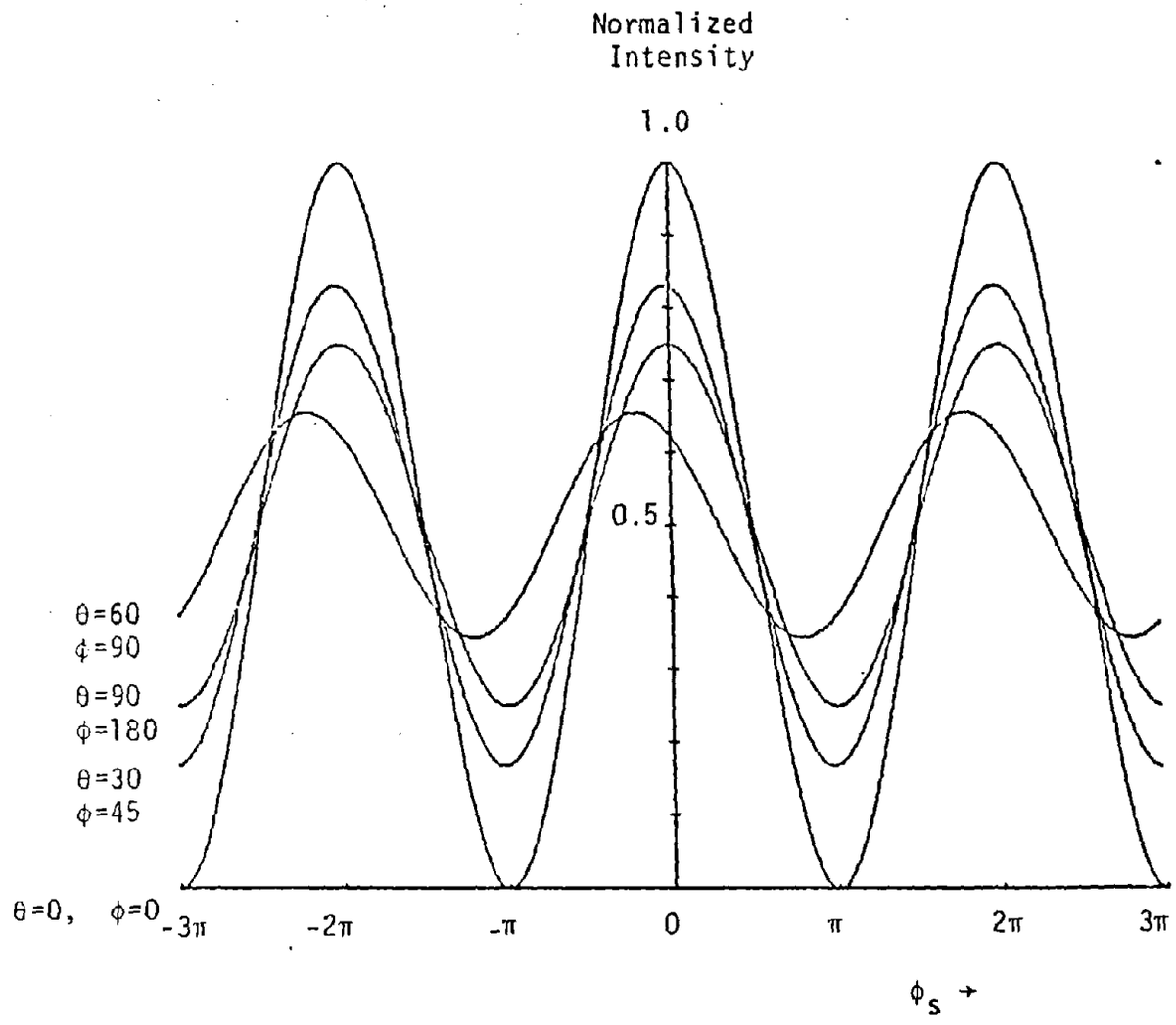

Fig. 7--Same as Fig. 3 except that input is partially polarized with degree of polarization P = 0.25 and no analyzer is used.

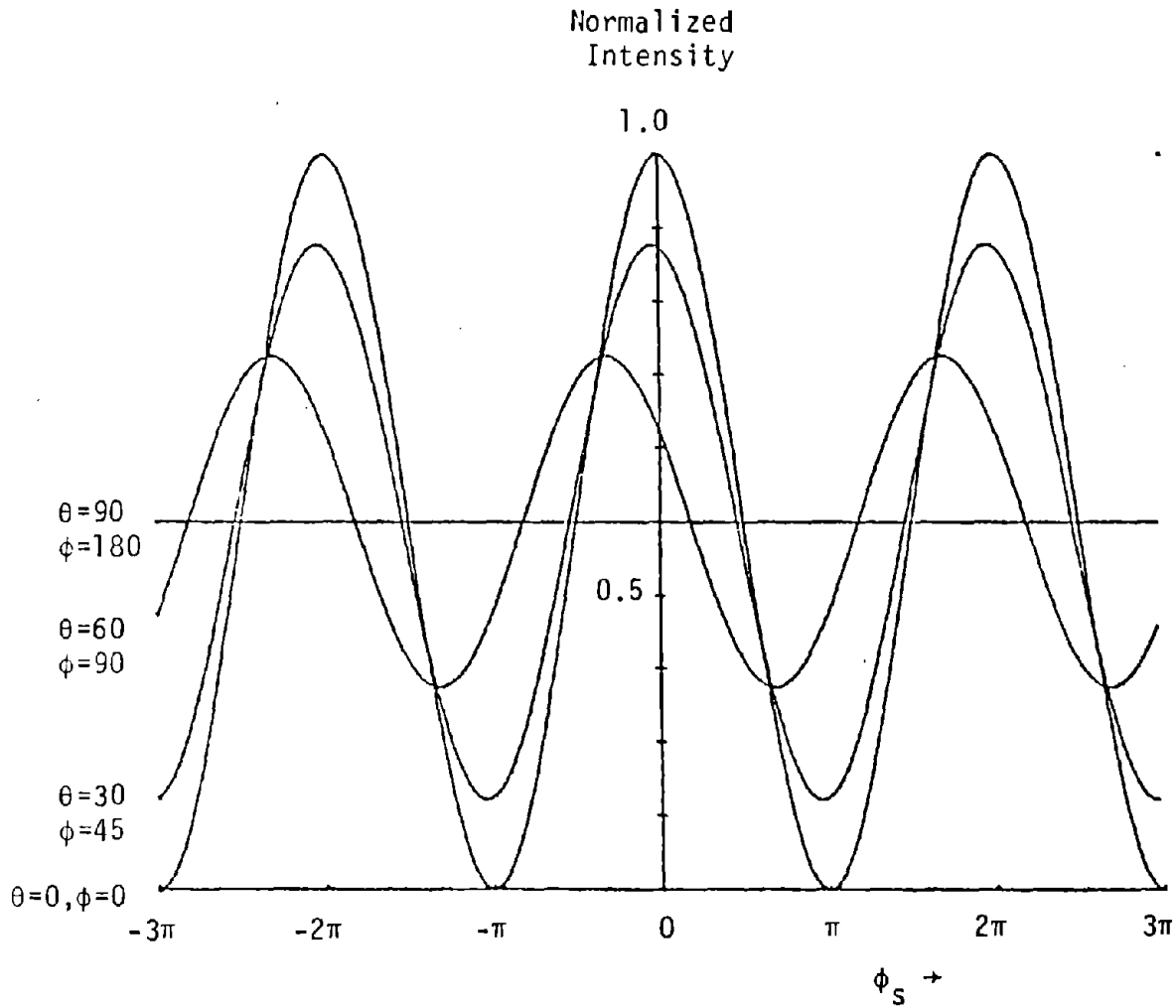

Fig. 8--Same as Fig. 7 except p = 0.50 .

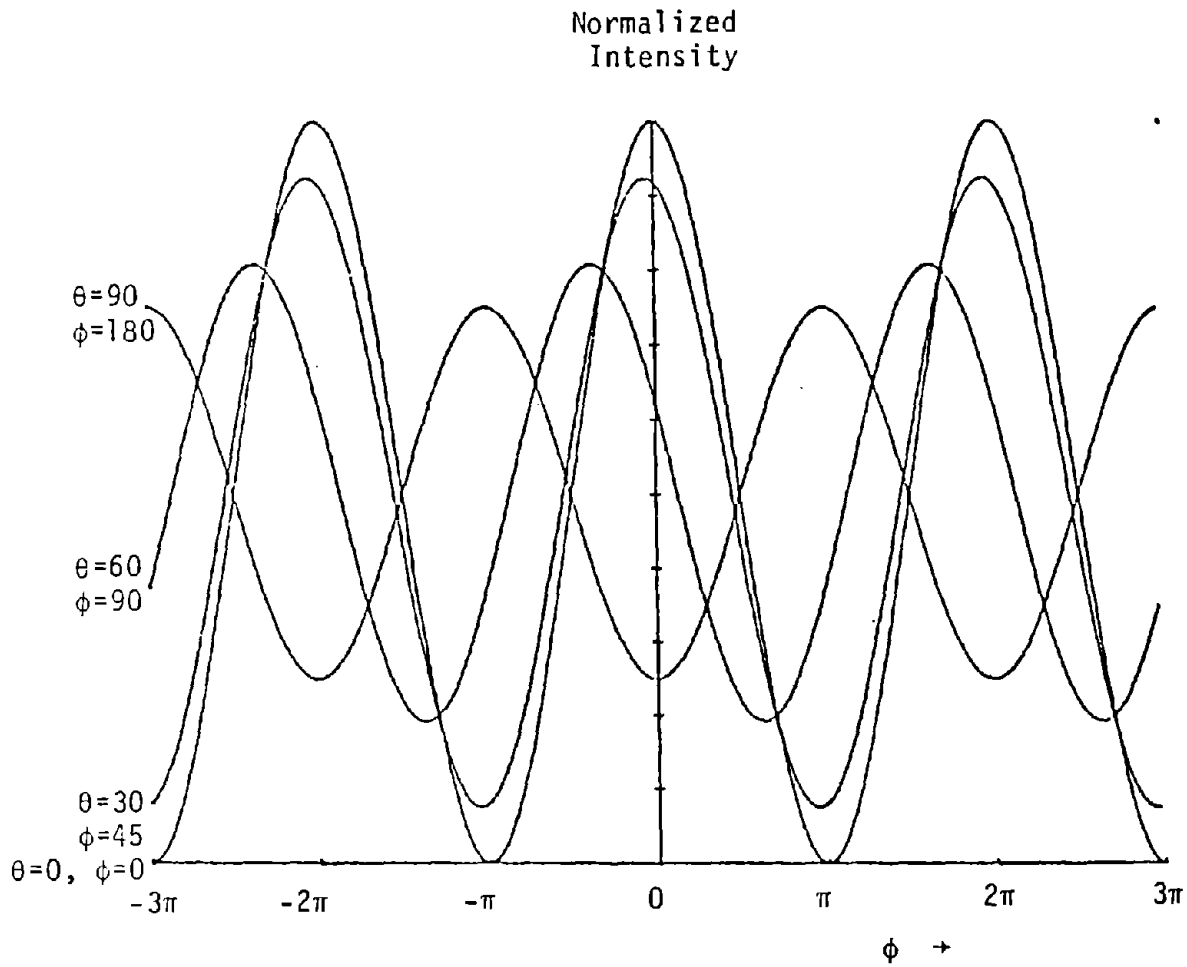

Fig. 9--Same as Fig. 7 except p = 0.75 .

Assume that the fiber maintains linear polarization but rotates the plane of polarization. Under this condition if the plane of polarization can be stabilized to $\pm$ 2.5 degrees, the maximum degree of polarization becomes 0.05 (5%) for a 3 deg/hr sensitivity.

The appendix contains explicit forms for the Jones matrices. It also contains a new formalism for the polarization analysis of FORS's using the coherency matrix. This formalism places the polarization analysis of FORS's on a firm theoretical foundation, and is especially useful for the case of partial polarization.

IV. EXPERIMENTS

Experiments have been performed using a CW fiber gyro with a single mode fiber of 600 m length and 1 m diameter, excited with a helium neon laser. Detector output current was displayed on an oscilloscope as a function of rotation rate of the system, giving patterns of the types plotted in Figs. 3 to 9. Environmental effects were simulated by subjecting a short length of fiber, inside the loop, to a double twist. Specifically, the fiber was clamped to the rotating table at two points spaced about 18" along the fiber. The fiber segment between the clamps contained slack, and a rotatable clamp was attached to the center of this segment, which could be rotated about the fiber axis. The fiber was twisted through an angle which produced approximately the maximum change in the displaced output pattern. This angle was generally in the range of 90° to 180°. The actual value was not important as the purpose was to confirm the qualitative predictions of the theory, which show some polarization states to be free of certain homogeneous environmental effects, while others are not.

Figure 10 is for the case of linear polarized input light together with a linear polarization filter at the detector, set to pass only the same polarization. The lower trace corresponds to zero twist angle and the upper trace results from introducing the twist. Note that the positions of the maxima and minima do not shift along the horizontal axis, confirming that recpirocity is satisfied. Note also that the peak amplitude does change, but that the amplitude of the minima does not, as predicted.

Figure 11 shows the results when the polarizer is rotated to pass only the polarization orthogonal to the input polarization, and Fig. 12 results when the polarizer is removed. Lower and upper traces are for the same twist states as before. Note in both cases the positions of maxima and minima shift horizontally as a function of twist, i.e., the system is nonreciprocal, and amplitude variation with twist is again present, all as predicted.

Figure 13 results when unpolarized light is used, and no polarizers are employed. The upper trace corresponds to zero twist, while the lower traces result when twist is introduced. Note that (1) the horizontal positions of the maxima and minima remain fixed and (2) the positions of the $\pi/2$ points remain fixed, again as predicted by the theory.

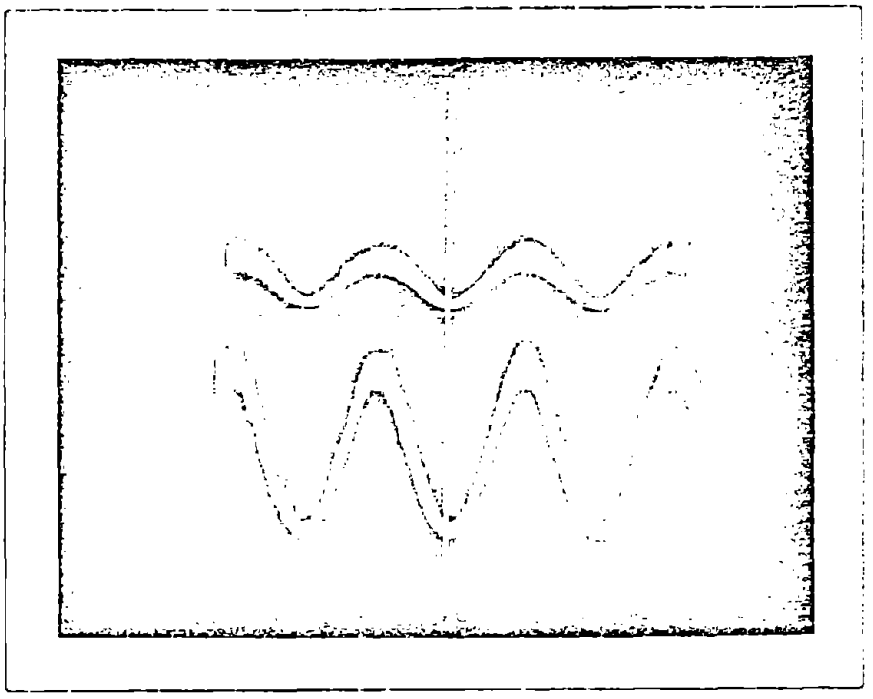

Fig. 10--Oscillogram of detector current (vertical axis) vs rotation rate (horizontal axis), for linear input polarization and co-polarized detector filter. Lower trace: fiber twist absent. Upper trace: fiber twist present.

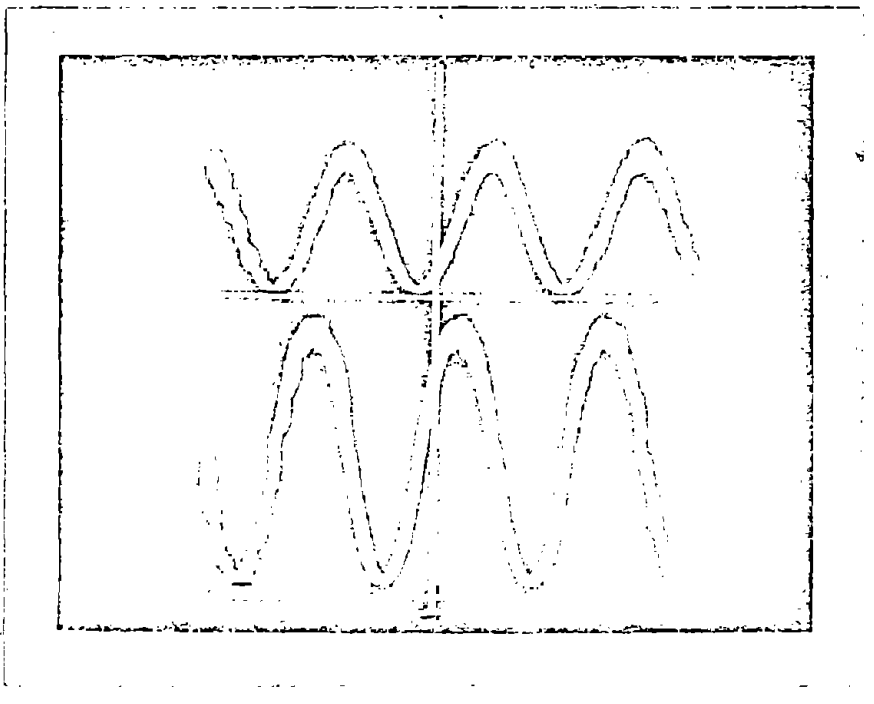

Fig. 11--Same as Fig. 10, except detector filter was cross-polarized.

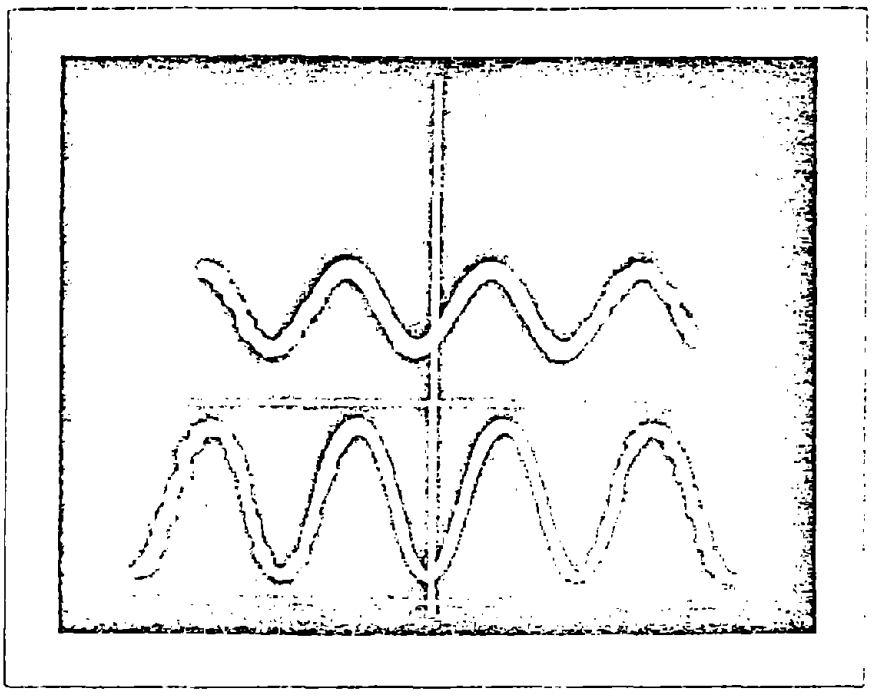

Fig. 12--Same as Fig. 10 except no detector polarization filter was used.

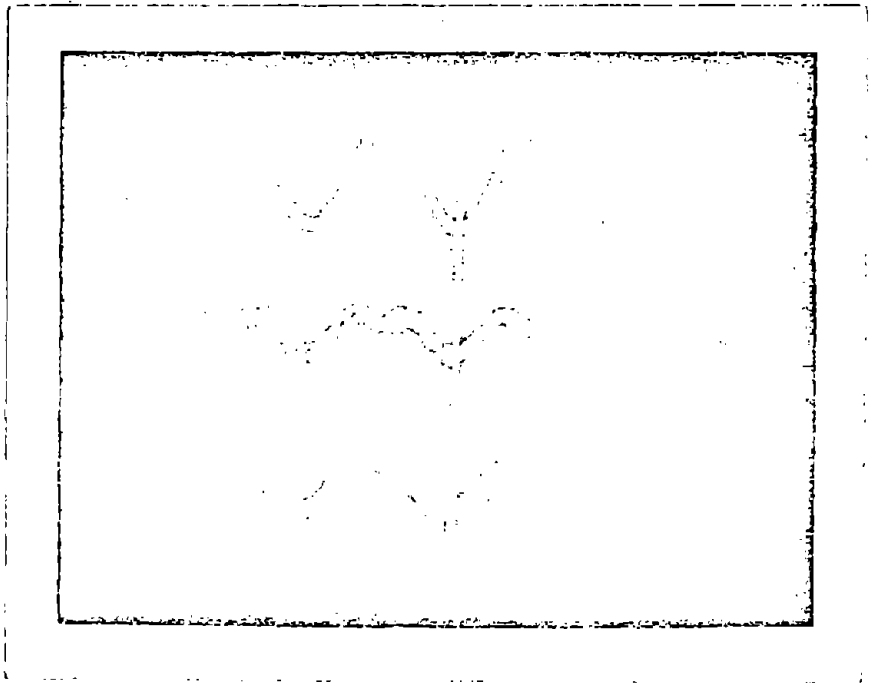

Fig. 13--Oscillogram of detector current (vertical axis) vs rotation rate (horizontal axis), for unpolarized input and no polarization filters. Upper trace: fiber twist absent. Lower traces: fiber twist present.

V. APPENDIX

We now consider first an explicit form for the Jones matrix for a real single mode fiber. Pictured schematically in Fig. A-1 is a real single mode fiber which propagates two polarization modes of propagation constants β_1 and β_2 respectively. At a point z along the fiber there exists a linear scattering center. This scattering center can exchange all or part of the powers in the two modes. At this point the Jones matrix T_{BA} can be represented as

$$T_{BA} = \begin{bmatrix} \cos\theta\, e^{j\phi_{11}} & \sin\theta\, e^{j\phi_{12}} \\ -\sin\theta\, e^{j\phi_{21}} & \cos\theta\, e^{j\phi_{22}} \end{bmatrix} \tag{19}$$

The Jones matrix T_{AB} can be obtained from T_{BA} by using the principle of reciprocity.

It now remains to specify the forms of the ϕ_{ij}'s . Here ϕ_{ij} represents the phase shift imparted to a wave which started in the j^{th} polarization and finished in the i^{th} polarization. By inspection of Fig. 1 we can write

$$\begin{aligned} &\text{(a)} \quad \phi_{11} = \beta_1 L \\ &\text{(b)} \quad \phi_{22} = \beta_2 L \\ &\text{(c)} \quad \phi_{12} = -\Delta\beta z + \beta_1 L \\ &\text{(d)} \quad \phi_{21} = \Delta\beta z + \beta_2 L \\ &\text{(e)} \quad \Delta\beta \equiv \beta_1 - \beta_2 \\ &\text{(f)} \quad \bar{\beta} = (\beta_1 + \beta_2)/2 \end{aligned} \tag{20}$$

By redefining the origin of phase (i.e., $\phi \to \phi - \bar{\beta}\, L$) we can write (19) as

$$T_{BA} \begin{bmatrix} \cos\theta\, e^{j\frac{\Delta\beta}{2} L} & \sin\theta\, e^{j\Delta\beta\left(\frac{L}{2} - z\right)} \\ \sin\theta\, e^{-j\Delta\beta\left(\frac{L}{2} - z\right)} & \cos\theta\, e^{-j\frac{\Delta\beta}{2} L} \end{bmatrix} \tag{21}$$

Finally we call $\Delta\beta L = \phi$ and $\Delta\beta\left(\frac{L}{2} - z\right) = \phi_{PD}/2$ (PD $\equiv$ path difference). The explicit forms for the $t_{k\ell}$'s are therefore

$$\begin{aligned} &(a) \quad t(x_2, x_1) = \cos\theta\, e^{j\phi} \\ &(b) \quad t(x_2, y_1) = \sin\theta\, e^{j\phi_{PD}} \\ &(c) \quad t(y_2, x_1) = -\sin\theta\, e^{j\phi_{PD}} \\ &(d) \quad t(y_2, y_1) = \cos\theta\, e^{j\phi} L \end{aligned} \tag{22}$$

For a fiber with N scattering centers the Jones matrix still has elements of the above form.

We next develop an alternative formulation of the effect of the optical fiber loop on FORS performance. Consider a wave of arbitrary polarization propagating in the z-direction, given by

$$E(z,t) = \begin{pmatrix} E_x \\ E_y \end{pmatrix} e^{j(\beta z - \omega t)} \tag{23}$$

The coherency matrix (J) is defined as

$$J \equiv \left\langle \vec{E}\, \vec{E}^{+} \right\rangle = \begin{bmatrix} \langle E_x E_x^* \rangle & \langle E_y E_y^* \rangle \\ \langle E_y E_x^* \rangle & \langle E_y E_y^* \rangle \end{bmatrix} \tag{24}$$

$\langle\ \rangle$: time average

$+$: hermitian conjugate

$\vec{E}\,\vec{E}^{+}$: dyadic product

$*$: complex conjugate

The intensity (I) of the wave represented by J is given as

$$I = \text{tr } J \tag{25}$$

The off-diagonal elements of J are the cross-correlation of the two polarization components. J is hermitian.

Examples of the coherency matrix for various polarized waves of unit intensity are as follows:

(a) Linear polarization in the x direction

$$J = \begin{bmatrix} 1 & 0 \\ 0 & 0 \end{bmatrix}$$

(b) Linear polarization at 45° to x-axis

$$J = \begin{bmatrix} 1/2 & 1/2 \\ 1/2 & 1/2 \end{bmatrix}$$

(c) Right-hand circular polarization

$$J = \begin{bmatrix} 1/2 & j/2 \\ -j/2 & 1/2 \end{bmatrix}$$

(d) unpolarized light

$$J = \begin{bmatrix} 1/2 & 0 \\ 0 & 1/2 \end{bmatrix}$$

(e) 50% partial polarized light-polarized part along x-axis

$$J = \begin{bmatrix} 3/4 & 0 \\ 0 & /14 \end{bmatrix}$$

For propagation of the coherency matrix through a linear systems, let the system be described by the matrix L, where L is defined by the relation

$$\vec{E}_{out} = L \vec{E}_{in} \tag{27}$$

The coherency matrix J_{out} is found from the coherency matrix J_{in} by the following expression

$$J_{out} = L J_{in} L^{+} \tag{28}$$

For a ring interferometer operated as a Sagnac rotation sensor, we can express L as (see Fig. 11):

$$L_{reciprocal} = P(T_{BS}T_{21}R_{BS} + R_{BS}T_{12}T_{BS}) \tag{29}$$

$$L_{nonreciprocal} = P(R_{BS}T_{21}R_{BS} + T_{BS}T_{12}T_{BS}) \tag{30}$$

P, T_{21}, T_{12} are as defined before and

$$R_{BS} = \begin{bmatrix} r_x & 0 \\ 0 & r_y \end{bmatrix} \qquad T_{BS} = \begin{bmatrix} t_x & 0 \\ 0 & t_y \end{bmatrix} \tag{31}$$

where r_x, r_y, t_x, t_y are complex valued transfer coefficients for the E-field.

To duplicate the results obtained earlier, set $R_{BS} = T_{BS} = I$ (the identity matrix). For cases 1, 2, and 3 use $J_{in} = \begin{bmatrix} 1 & 0 \\ 0 & 0 \end{bmatrix}$. For case 4 use $J_{in} = \begin{bmatrix} 1 & 0 \\ 0 & 1 \end{bmatrix}$ and for case 5 use $\begin{bmatrix} \frac{1}{2}(1-P) & 0 \\ 0 & \frac{1}{2}(1+P) \end{bmatrix}$ where P is the degree of polarization of the wave..

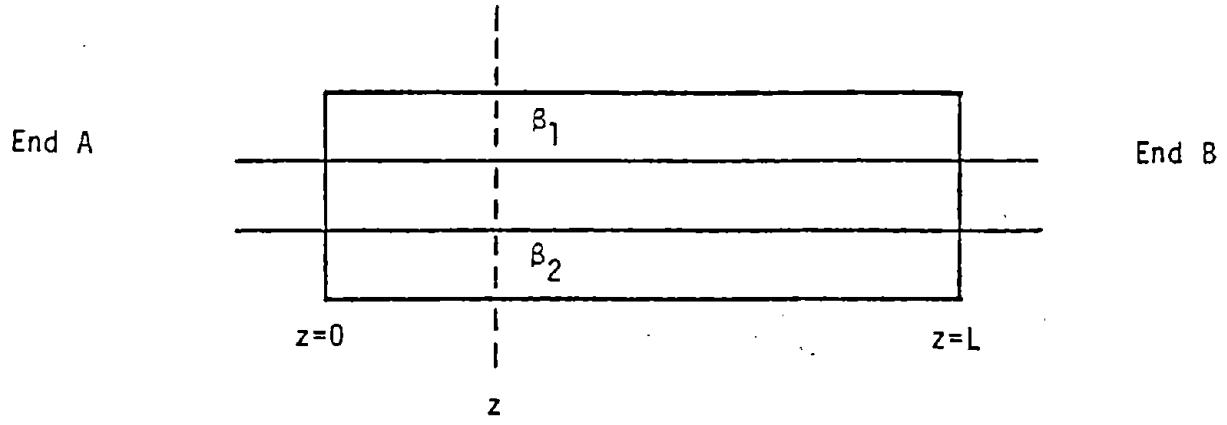

Fig. 10--Real single mode fiber.

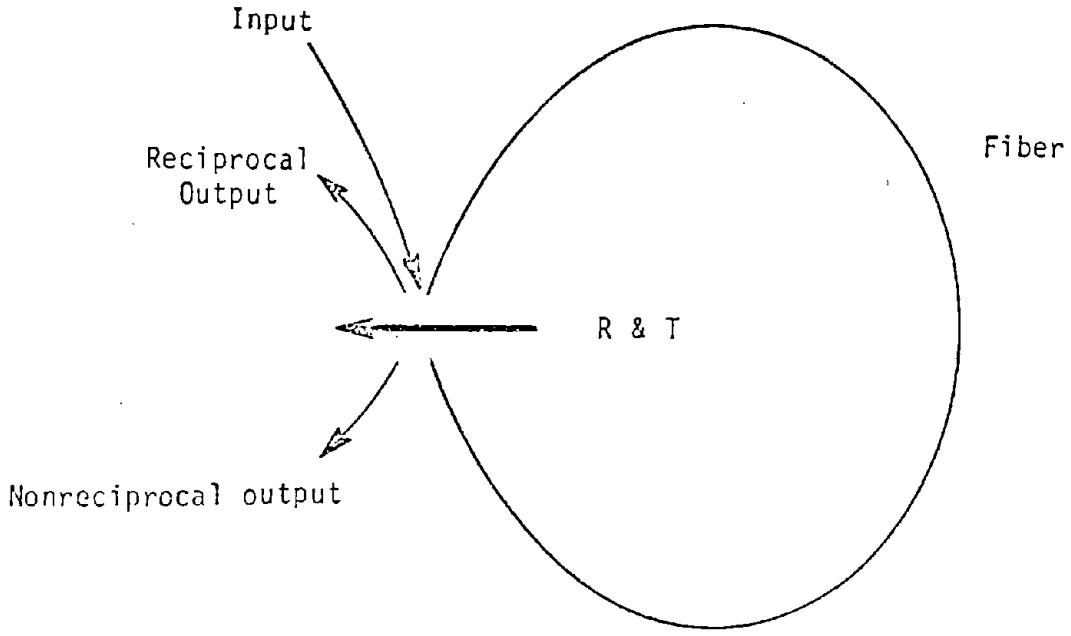

Fig. 11--Reciprocal and nonreciprocal ports of the FORS.

REFERENCES

1. V. Vali, R.W. Shorthill and M.F. Berg, Appl. Optics 16, 10 (1977).
2. V. Vali and M.F. Berg, SPIE Proceedings 157, p.
3. Raymond Goldstein and Willis C. Goss, SPIE Proceedings 157, p.
4. M.N. McLandrich and E.H. Rast, SPIE Proceedings 157, p.
5. J.I. Davis and S. Ezekiel, SPIE Proceedings 157, p.
6. H. Arditty, H.J. Shaw, M. Chodorow and R. Kompfner, SPIE Proceedings 157, p.
7. D.E. Thomson, D.B. Anderson, S.K. Yao and B.R. Youmans, Appl. Phys. Lett. 33 (1978).
8. R.F. Cahill and E. Udd, Optics Lett. 4,3 (1979).
9. R. Ulrich, Optics Lett. 5, 5 (1980).
10. W.C. Goss, R. Goldstein, M.D. Nelson, H.T. Fearnebaugh and O.G. Ramer, Appl. Optics 15, 16 (1980).
11. E.J. Post, Rev. Mod. Phys., 19, 2, 475 (1967).
12. R. Ulrich and M. Johnson, Optics Lett., 4, 5 (1979).
13. R.H. Stolen, V. Ramaswamy, P. Kaiser and W. Pleibel, Appl. Phys. Lett., 13, 699 (1978).
14. R. Ulrich, Appl. Phys. Lett. 35, 11 (1979).
15. $p = \sqrt{1 - 4 \frac{\det[J]}{[\mathrm{tr}\ J]^2}}$ where J is the coherency matrix of the wave (see Born and Wolf, Principles of Optics).

APPENDIX B

COHERENCE MATRIX FORMULISM

The description of the polarization of a light wave requires the specification of its state and degree of polarization. The coherence matrix[1] of the light wave contains this information. Any two orthonormal polarization states can be used as the basis for the coherence matrix. For the analysis performed in this appendix, the two states are chosen as linearly polarized waves along the x and y axes. Let E_x and E_y be the instantaneous projections of the electric field, E, of the light wave along the x axis and y axes respectively. The coherence matrix J of the light wave is given in Eq. (1).

$$J = \begin{pmatrix} \langle E_x \; E_x^* \rangle & \langle E_x \; E_y^* \rangle \\ \langle E_y \; E_x^* \rangle & \langle E_y \; E_y^* \rangle \end{pmatrix} \tag{1}$$

The brackets $\langle \; \rangle$, signify the infinite time average and the asterisks signify the complex conjugate. There are several properties of the coherence matrix which are useful. The first property is that the intensity (I) of the light wave is the trace of the coherence matrix. Second, the coherence matrix is hermitian and third, the degree of polarization (P) of the light wave can be calculated from the eigenvalues $(\lambda_1 \; , \lambda_2)$ of the coherence matrix. These properties are summarized in Eq. (2).

$$\begin{aligned} I &= \mathrm{Tr}J \\ J_{kl} &= J_{lk}^* \\ P &= |\lambda_1 - \lambda_2|/(\lambda_1 + \lambda_2) \end{aligned} \tag{2}$$

The coherence matrices for various states and degrees of polarization are shown in Fig. 1. Linear polarization along the x axis and the y axis form the basis set for these coherence matrices. The off-diagonal terms of the coherence matrix represent the correlation between the fields along the basis vectors.

Suppose that we have a black box as shown in Fig. 2. A light wave characterized by $\vec{E}_{in} = (E_x, E_y)_{in}$ is input into the box. The output light wave from the box is characterized by $\vec{E}_{out} = (E_x, E_y)_{out}$. If the box contains only linear components, the output can be related to the input by a 2×2 matrix, S, of complex numbers. The mathematical relation is given in Eq. (3).

$$\vec{E}_{out} = S \vec{E}_{in} \quad . \tag{3}$$

If the input and output fields are related by Eq. (3), it is easy to show that the input and output coherence matrices are related by the formula in Eq. (4) where S^+ represents the hermitian adjoint of S.

$$J_{out} = S J_{in} S^+ \quad . \tag{4}$$

Equation (4) is valid only if the matrix S describing the linear system does not change appreciably during the interval of time over which the time averages contained in J are taken. It is also easy to show that if two light waves with coherence matrices J_1 and J_2 are superimposed, the coherence matrix of the total light wave is just the sum of the coherence matrices of each light wave.

This formalism is an important advance because it can be used to treat quasi-monochromatic light (i.e., light with degree of polarization other

a) $J = \begin{pmatrix} 1 & 0 \\ 0 & 0 \end{pmatrix}$ Linearly polarized along X axis

b) $J = \begin{pmatrix} 0 & 0 \\ 0 & 1 \end{pmatrix}$ Linearly polarized along Y axis

c) $J = \frac{1}{2}\begin{pmatrix} 1 & 1 \\ 1 & 1 \end{pmatrix}$ Linearly polarized at 45 to X axis

d) $J = \frac{1}{2}\begin{pmatrix} 1 & j \\ -j & 1 \end{pmatrix}$ Right hand circular polarization

e) $J = \frac{1}{2}\begin{pmatrix} 1 & -j \\ j & 1 \end{pmatrix}$ Left hand circular polarization

f) $J = \frac{1}{2}\begin{pmatrix} 1 & 0 \\ 0 & 1 \end{pmatrix}$ Unpolarized light

g) $J = \frac{1}{2}\begin{pmatrix} 3/4 & 0 \\ 0 & 1/4 \end{pmatrix}$ Partially polarized light with polarized part being linearly polarized along X axis. Degree of polarization is 1/2.

Figure 1. Coherence matrices for various states and degrees of polarization.

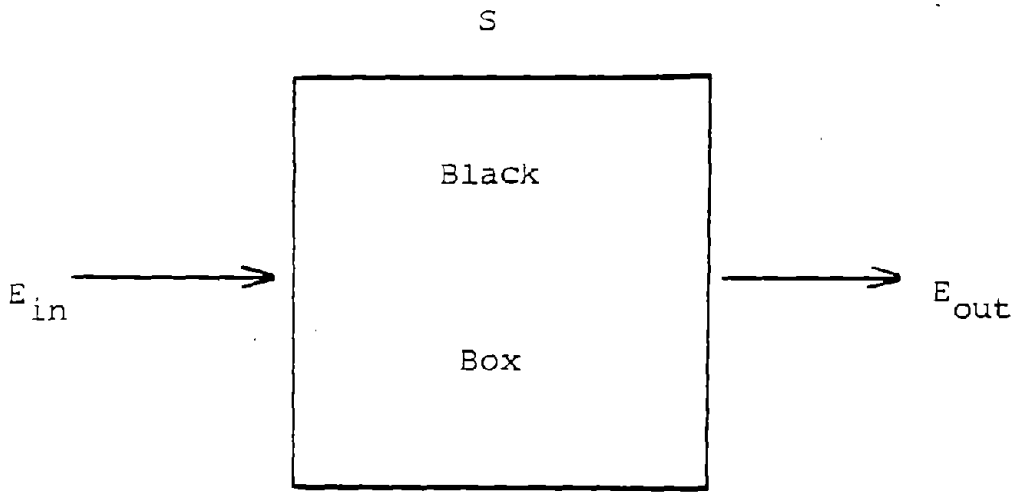

$$E_{out} = SE_{in}$$

Figure 2. A linear system is represented as a black box by its transfer matrix, S. The transfer matrix relates the output vector to the input vector.

than unity). Previous formalisms[2] could treat only completely polarized light. The analysis of the unpolarized fiber gyro is greatly facilitated by this formalism.

APPENDIX B - REFERENCES

1. E. Born and M. Wolf, Principles of Optics: Electro-magnetic Theory of Propagation, Interference and Diffraction of Light, Pergamon Press, New York, 1980, 6th Edition, p. 267.
2. R. Ulrich and M. Johnson, "Fiber-ring Interferometer: Polarization Analysis," Optics Letters 4, 152-154 (1979).

APPENDIX C

JONES MATRICES FOR BIREFRINGENT, SINGLE MODE FIBER GYROS

The birefringence of single mode fiber gyros is described by Jones matrices. This appendix develops Jones matrices for the optical fiber, the polarizer, and the beamsplitter. The Jones matrix of the fiber gyro can be expressed in terms of the Jones matrices of the components.

Describing an optical fiber by Jones matrices is equivalent to modeling the optical fiber as a general four port, linear system as shown in Fig. 1 with the four ports and the paths between the ports depicted explicitly. Each path is characterized by a complex scattering coefficient. The complex scattering coefficient describes the phase shift collected by the light wave and the amplitude of the light wave which travels a specific channel through the system. The scattering coefficients are dimensionless. We can write a Jones matrix S_{12} for propagation from end number 2 to end number 1 of the fiber and a Jones matrix S_{21} for propagation in the opposite direction. The principle of reciprocity relates the complex scattering coefficients. The representation of the matrices S_{12} and S_{21} in terms of the complex scattering coefficients are presented in Eqs. (1a) and (1b). Equation (1c) shows the relation between the complex scattering coefficients as a result of reciprocity.

$$S_{12} = \begin{pmatrix} t(x1,x2) & t(x1,y2) \\ t(y1,x2) & t(y1,y2) \end{pmatrix} \qquad (1a)$$

$$S_{21} = \begin{pmatrix} t(x2,x1) & t(x2,y1) \\ t(y2,x1) & t(y2,y1) \end{pmatrix} \qquad (1b)$$

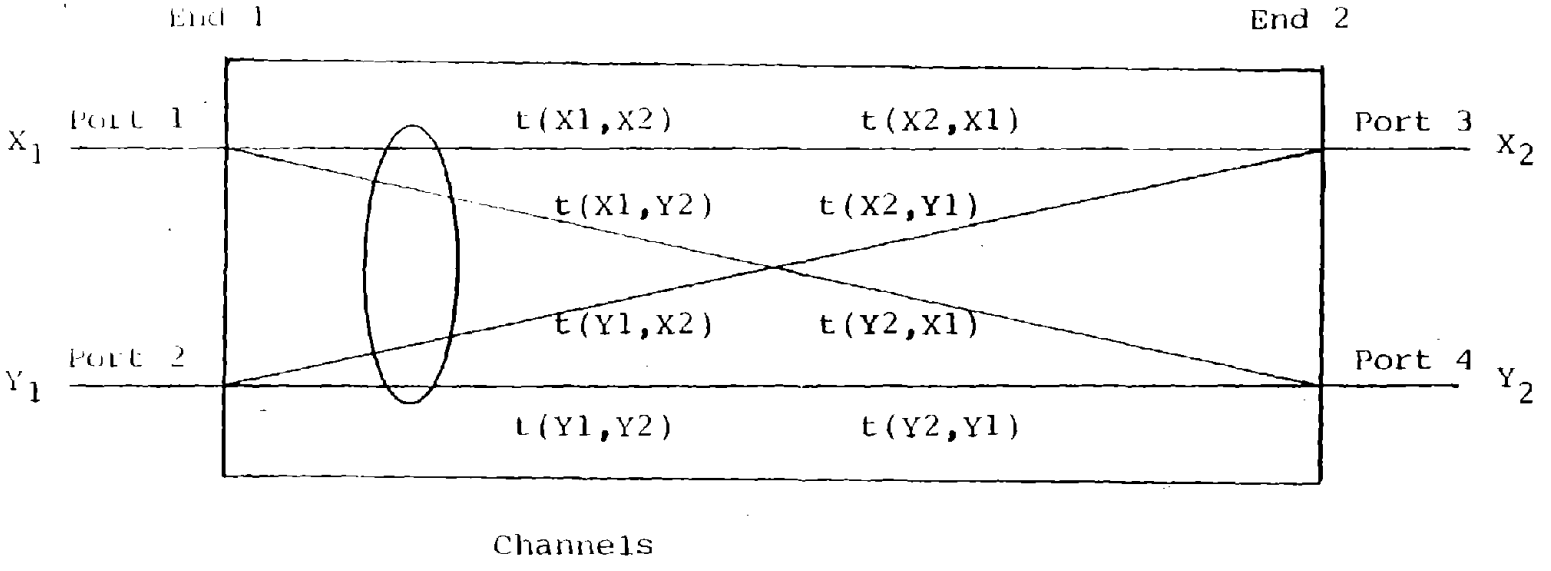

Figure 1. Representation of an optical fiber as a general four port linear system. The four ports, the channels, and the complex scattering coefficents are explicitly shown. The scattering coefficents represent the effect of a channel on a light wave which propagates along that channel.

$$t(k,\ell) = t(\ell,k) \qquad (1c)$$

$$k,\ell = x1,x2,y1,y2$$

Equation (1c) means that the direction in which a path is transversed does not matter. For a lossless fiber, the matrices S_{12} and S_{21} are unitary. This means that the sum of the absolute squares of the elements in any row or column is equal to 1. Loss can be introduced by multiplying the matrices S_{12} and S_{21} by $e^{-\alpha L}$, where L is the length of the fiber and α is the loss per unit length of the fiber. In the analysis of the polarization properties of various fiber optic rotation sensors (FORS), it is assumed that the fibers are lossless. The Sagnac phase shift modifies the matrices S_{12} and S_{21} as shown in Eqs. (2a) and (2b).

$$S_{12} = e^{+j\phi_s/2} \begin{pmatrix} t(x1,x2) & t(x1,y2) \\ t(y1,x2) & t(y1,y2) \end{pmatrix} \qquad (2a)$$

$$S_{21} = e^{-j\phi_s/2} \begin{pmatrix} t(x2,x1) & t(x2,y1) \\ t(y2,x1) & t(y2,y1) \end{pmatrix} \qquad (2b)$$

ϕ_s is the Sagnac phase shift.

Although the matrices S_{12} and S_{21} can be used as given in Eq. (2a) and (2b), it will simplify further analysis if an explicit form is given for the $t(k,\ell)$'s. The $t(k,\ell)$'s are complex numbers which represent the effect of a channel on a light wave, propagating from one port to another port in the system. They will be represented in polar forms. The magnitude of $t(k,\ell)$ is the amplitude of the electric field of the light wave, at port k for unit electric field applied at port 1. The phase of $t(k,\ell)$ is the

phase shift undergone by a light wave traveling the channel from port ℓ to port K. The 2 x 2 matrix of the $t(k,\ell)$'s is unitary. Using this fact, the $t(k,\ell)$'s can be written in the following polar forms.

$$t(x1,x2) = \cos\theta.\ \exp[j\emptyset(x1,x2)] \quad (3a)$$

$$t(x1,y2) = \sin\theta.\ \exp[j\emptyset(x1,y2)] \quad (3b)$$

$$t(y1,x2) = -\sin\theta.\ \exp[j\emptyset(y1,x2)] \quad (3c)$$

$$t(y1,y2) = \cos\theta.\ \exp[j\emptyset(y1,y2)] \quad (3d)$$

In Eqs. (3a), (3b), (3c), (3d), the parameter θ describes the rotation of the input state of polarization by the fiber. The phase shifts $\emptyset(k,\ell)$ must now be determined by considering a length L of optical fiber with a single scattering point located at a distance Z along the fiber. This model is shown in Fig. 2. The phase shifts $\emptyset(k,\ell)$ calculated from this model are given in Eq. (4).

$$\emptyset(x1,x2) = \beta_x L \quad (4a)$$

$$\emptyset(y1,y2) = \beta_y L \quad (4b)$$

$$\emptyset(x1,y2) = \beta_y L + \Delta\beta Z \quad (4c)$$

$$\emptyset(y1,x2) = \beta_x L - \Delta\beta Z \quad (4d)$$

$$\Delta\beta = \beta_x - \beta_y \quad (4e)$$

These equations can be put in a more symmetric form by factoring out the term $(\beta_x + \beta_y)L/2$. This results in the following equations for the phase shifts:

$$\emptyset(x1,x2) = \bar{\beta} L + \Delta\beta L/2 \quad (5a)$$

$$\emptyset(y1,y2) = \bar{\beta} L - \Delta\beta L/2 \quad (5b)$$

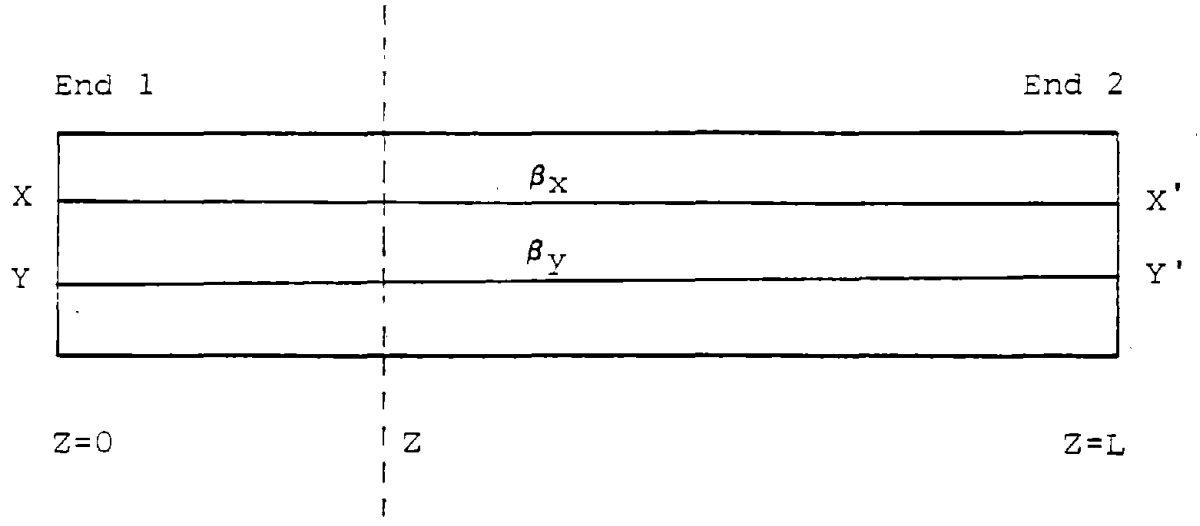

Figure 2. Schematic representation of a single mode fiber. The paths taken by the two polarizations X,Y are shown explicitly by XX' and YY' with propagation constants β_x and β_y . Z can represent a point in the fiber were the power in the two modes is interchanged.

$$\phi(x1,y2) = \bar{\beta}\, L - \Delta\beta(L/2 - Z) \tag{5c}$$

$$\phi(y1,x2) = \bar{\beta}\, L + \Delta\beta(L/2 - Z) \tag{5d}$$

$$\bar{\beta} = (\beta_x + \beta_y)/2 \tag{5e}$$

combining Eqs. (2), (3), and (4), an explicit representation for the matrices S_{12} and S_{21} is found for the case of a fiber with a single scattering center.

$$S_{12} = e^{j\phi_s/2}\, e^{j\bar{\beta}L} \begin{pmatrix} \cos\theta\, e^{j\Delta\beta L/2} & \sin\theta\, e^{-j\Delta\beta(L/2-Z)} \\ -\sin\theta\, e^{+j\Delta\beta(L/2-Z)} & \cos\theta\, e^{-j\Delta\beta L/2} \end{pmatrix} \tag{6a}$$

$$S_{21} = e^{-j\phi_s/2}\, e^{j\bar{\beta}L} \begin{pmatrix} \cos\theta\, e^{j\Delta\beta L/2} & -\sin\theta\, e^{+j\Delta\beta(L/2-Z)} \\ \sin\theta\, e^{-j\Delta\beta(L/2-Z)} & \cos\theta\, e^{-j\Delta\beta L/2} \end{pmatrix} \tag{6b}$$

In general a real fiber has many scattering points. To find the matrices S_{12} and S_{21} in this case, divide the fiber into sections, each section containing one scattering point, then multiply the matrices for each section together to get the matrix for the fiber. The matrices S_{12} and S_{21} have the same general form as the matrices in Eqs. (6a) and (6b). This general form is

$$S_{12} = e^{j\phi_s/2}\, e^{j\bar{\phi}(L)} \begin{pmatrix} \cos\theta\, e^{+j\xi(L)/2} & \sin\theta e^{-j\phi(L)/2} \\ -\sin\theta\, e^{j\phi(L)/2} & \cos\theta\, e^{-j\xi(L)/2} \end{pmatrix} \tag{7a}$$

$$S_{21} = e^{-j\phi_s/2}\, e^{j\bar{\phi}(L)} \begin{pmatrix} \cos\theta\, e^{+j\xi(L)/2} & -\sin\theta\, e^{j\phi(L)/2} \\ \sin\theta\, e^{-j\phi(L)/2} & \cos\theta\, e^{-j\xi(L)/2} \end{pmatrix} \tag{7b}$$

In Eqs. (7a) and (7b) $\bar{\emptyset}(L)$ is an average phase shift which depends on the length of the fibers; ξ and $\emptyset$ are phase shifts which depend on the birefringence and number of scattering centers in the fiber. The physical interpretations of ξ and $\emptyset$ are as follows: $\emptyset$ is the nonreciprocal phase shift introduced by the fiber and its value is the phase difference between light waves which travel from port x1 to y2 and from port x2 to port y1 (see Fig. 1 of Appendix C); ξ is the measure of the birefringence of the fiber and its value is the phase difference between light waves which travel from port x1 to port x2 and from port y1 to y2.

In order to fully represent a fiber gyro, it is necessary to develop Jones matrices for polarizers and beam splitters. The Jones matrix P, for a general polarizer at an angle a to the x-axis is given in Eq. (8).

$$P = \begin{pmatrix} p_x\cos^2 a + p_y\sin^2 a & (p_x-p_y)\ (\sin a)\ (\cos a) \\ (p_x-p_y)\ (\sin a)\ (\cos a) & p_x\sin^2 a + p_y\cos^2 a \end{pmatrix} \qquad (8)$$

In this expression, p_x and p_y are the fractions of the x,y electric fields passed by the polarizer. For an ideal polarizer $p_x = 1$ and $p_y = 0$. The basis polarizations for this representation of a polarizer are the x and y linear polarizations.

A beam splitter is characterized by two Jones matrices, one for transmission (T) and one for reflection (R). The form of these matrices is dependent on the particular basis polarizations chosen. For an ideal, lossless, 50-50 beam splitter in the x and y linear polarization basis, the T and R matrices are given in Eqs. (9a) and (9b).

$$T = \begin{pmatrix} \frac{1}{\sqrt{2}}\, e^{j\pi/4} & 0 \\ 0 & \frac{1}{\sqrt{2}}\, e^{j\pi/4} \end{pmatrix} \qquad (9a)$$

$$R = \begin{pmatrix} \frac{1}{\sqrt{2}} e^{-j\pi/4} & 0 \\ 0 & \frac{1}{\sqrt{2}} e^{-j\pi/4} \end{pmatrix} \qquad (9b)$$

The T and R matrices which represent a real beamsplitter in the x and y linear polarization basis are given in Eqs. (10a) and (10b).

$$T = \begin{pmatrix} t_x & 0 \\ 0 & t_y \end{pmatrix} \qquad (10a)$$

$$R = \begin{pmatrix} r_x & 0 \\ 0 & r_y \end{pmatrix} \qquad (10b)$$

In Eqs. (10a) and (10b), t_x , t_y , r_x and r_y are complex numbers with $|t_x|^2 + |r_x|^2 = 1$ and $|t_y|^2 + |r_y|^2 = 1$.

With the Jones matrices and the coherence matrix formalism (Appendix A) it is possible to analyze various types of fiber gyros. The birefringence inherent in all single mode optical fibers can now be described by three measurable quantities θ , ϕ , and ξ . This can result in better characterization of fiber birefringence and the effects of fiber birefringence on fiber gyroscopes.

APPENDIX D

GL 3150

Limitation of rotation sensing by scattering

C. C. Cutler, S. A. Newton, and H. J. Shaw

Edward L. Ginzton Laboratory, W. W. Hansen Laboratories of Physics, Stanford University, Stanford, California 94305

Received July 16, 1980

There appear to be limitations in the operation of optical-fiber Sagnac gyro rotation sensors that have imposed a minimum measurable rotation rate that is much higher than that caused by quantum noise. We show that one source of limitation, namely, the superposition of a nonreciprocal pair of waves generated by backward scattering from the incident waves, can result in significant error but can be mitigated by appropriate system design and signal modulation.

Fiber gyro progress is now on a plateau at which the observed sensitivity is far below the expected range. Calculations of the sensitivity of the system, assuming no noise sources other than basic quantum noise, indicate a capability for performance extending to less than 10^{-3} degree of rotation per hour.[1] In spite of the attractive promise, no experimental fiber gyro has come close to this level. Noise, in the range of 10^3 to 10^6 times higher than quantum noise, is found to be present. The noise is sufficient to limit the sensitivity to the range of 1.0 to 100 deg/h, even with integration times extending to many seconds.[2-7] Existing analyses of the system, covering all presumed sources of noise, indicate no unavoidable sources that have a magnitude sufficient to change the predicted sensitivity. In this Letter, we identify an effect, the consequences of which have not been treated, give estimates of its magnitude, and propose new practical approaches to its solution.

Reciprocal and Nonreciprocal Effects

The factors that previously have been recognized as limiting the accuracy of rotation measurement are, broadly, residual nonreciprocal characteristics in the light path, nonhomogeneous environmental changes, quantum noise in the conversion of light to electrical signals, and electrical noise in the measuring system. The requirement of optical reciprocity in the two waves has dictated the use of single-mode fiber, in order to ensure that there are identical paths in the two directions,[8,9] and precise environmental control of inhomogeneous vibration and temperature changes.[10] Quantum noise and electrical noise have been considered,[11] and there appear to be adequate sources, fibers, and detectors for the precise measurement of phase. Scattered radiation that is due to inhomogeneities in the fiber produces a secondary pair of waves propagating in the fiber. These secondary waves and the mechanisms producing them are rather well known. However, we find that in the Sagnac interferometer these same waves can produce interfering components in the output that, in the absence of conditions that randomize their phase, could have an order of magnitude consistent with existing sensitivity limitations. The backscattered waves, as viewed at the output of the loop, do not share the property of reciprocity possessed by the original incident waves and can contain a component that cannot be treated merely as white noise.

At least the parts of the scattered waves that are due to physical defects in the fiber and to Rayleigh scattering are, to some degree, temporally and spatially coherent with the two primary waves and add vectorially at unpredictable phases that are not identical for the two waves (Fig. 1). If the source and the system were absolutely stable, the error that was due to the secondary waves would be constant and could be calibrated without limiting the sensitivity or accuracy of the system. Conversely, if conditions were sufficiently variable, coherence could be completely destroyed, and the waves would simply contribute shot noise, as has previously been assumed. In fact, however, if left alone, the secondary waves could produce an unpredictable error much larger than shot-noise contributions.

The forward scattering appears to have little effect on the uncertainty in phase and is believed to be reciprocal, affecting the oppositely directed waves alike. The part of the scattered radiation that falls within the acceptance angle of the fiber in the reverse direction, however, provides the secondary waves that interfere with the desired (primary) counterpropagating waves.

Quantitative Evaluation

An estimate of the magnitude of phase uncertainty in a fiber loop can be made from simple calculations. As an example, consider an attenuation $\exp(-\alpha_s L)$ that is due to Rayleigh scattering with the lost energy uniformly scattered over the length of a fiber with a scattering directivity G along the fiber. The fraction of the total scattered energy that is captured by the fiber core is $G\beta^2/4$, where[12] β is the acceptance angle of the fiber core and $1 < G < 1.5$. The detailed values of G and other parameters in this Letter may depart from the values assumed, depending on various factors, but this departure will not change the order of magnitude of our conclusions.

For a loop length L, it can easily be shown that, for small attenuation, the ratio of the power in the backscattered secondary wave to that in the primary wave after one circulation is given by

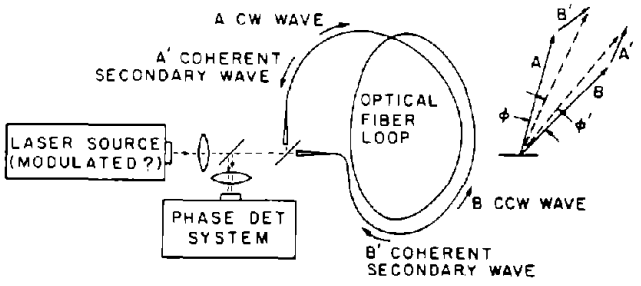

Fig. 1. Fiber-loop Sagnac interferometer. The scatter loss in a fiber that is due to fixed scattering centers, including Rayleigh scattering (the principal loss mechanism in very-low-loss fibers), gives rise to counterrotating secondary waves that are indistinguishable from the signal component that is caused by rotation. Their cumulative effect can be reduced by suitably modulating the input signal. ϕ, phase change that is due to rotation rate. ϕ', phase change including the secondary wave vectors.

Table 1. Parameters for Numerical Estimate

Symbols	Parameters	Values Used
λ	Wavelength	1.0 μm
c	Free-space velocity of light	3×10^8 msec
n	Refractive index of fiber	1.5
N	Number of turns in length L	318
D	Loop diameter	1.0 m
β	Capture angle of fiber	0.1 rad
G	Directional gain	1.0
α_s	Attenuation constant	1.2×10^{-4} m^{-1} ($\sim$0.5 dB/km)
L	Fiber length	1000 m

$$P_s/P_1 \simeq 1/4G\beta^2\alpha_s L. \tag{1}$$

The two counterrotating pairs of waves can combine to give a maximum phase deviation of

$$\phi_{max} = 2(P_s/P_1)^{1/2} = \beta(G\alpha_s L)^{1/2}, \tag{2}$$

which, for any single measurement, is indistinguishable from a phase shift induced by rotation. The rotation rate that corresponds to this phase deviation is obtained using the well-known Sagnac formula and is given by

$$\Omega_{max} = \frac{\lambda c}{2N(\pi D)^2}\beta(G\alpha_s L)^{1/2}, \tag{3}$$

or, substituting $N = L/(\pi D)$,

$$\Omega_{max} = \frac{\lambda c\beta}{2\pi D}\left(\frac{G\alpha_s}{L}\right)^{1/2}. \tag{4}$$

Using the values given in Table 1 for a single transit around a multiturn loop, we calculate a maximum phase error of 0.035 rad that linearly translates to a rotation error of up to 0.095 deg/sec or 341 deg/h.

Minimization of Error Due to Scattering

There are a number of ways in which the coherence between the primary and secondary (scattered) waves may be reduced. Some ways may reduce the reciprocity of the two primary waves, but some, such as frequency modulation of the primary signal or a physical modulation of the loop length in a controlled fashion, may not. If we assume such a modulation at a level high enough so that the number of wavelengths in the loop is changed significantly in the sampling time, the secondary waves add to the emerging primary waves with random phase. If we sample at a frequency of M per unit of time, and if the secondary wave phase is random between samples, the uncertainty in the angular position of the interferometer after a given time is determined by a random-walk process and is given by

$$\theta = M^{-1/2}\Omega_{rms} \simeq (2M)^{-1/2}\Omega_{max}. \tag{5}$$

In the foregoing example, taking 10 samples/sec and integrating for a full hour would yield a random-walk rotation error of 1.27 deg/h$^{1/2}$. This error is of the same order of magnitude as that of the best operation yet reported.[2-7]

The error that is due to scattering is probably lessened somewhat in existing fiber gyros because of certain factors (some inadvertent, some unavoidable) that act to reduce the coherence between the primary and secondary waves. The systems referred to above use modulation, which may serve to randomize the phase of the scattered waves to some extent, although the modulation is employed for a basically different purpose. Some degree of randomness undoubtedly occurs because of mechanical and thermal changes, but the changes produce other errors if they are not completely and instantaneously reciprocal. Variation in laser frequency is another source of randomization.

These factors notwithstanding, the contribution of backscattering to the overall error may still be significant or even dominant. Furthermore, as the sensitivity of these systems to mechanical and thermal perturbations is reduced, an increase in the coherence of the scattered waves is expected, since the effects of the remaining environmental variations are in general too slow to permit independent random sampling at frequencies high enough to reduce significantly the error that is due to scattering. How rapidly can we sample and expect to have the secondary (scattered) waves uncorrelated in phase? It will take additional analysis to determine the limits, but it seems probable that the effects of the secondary waves can be made very small. For instance, if we use a pulsed system, with pulses introduced at a rate c/nL (i.e., pulse length = transit time), and shift the pulses in frequency by c/nL per period [which is $(c/nL)^2$ per second] to randomize the phase of the scattered wave, then $M = 2 \times 10^5$ per second. The error that is due to Rayleigh scattering alone becomes 0.00015 deg/sec$^{1/2}$ (1-sec random walk) or 0.009 deg/h$^{1/2}$ (1-h random walk). For the 1-km fiber, this requires a 200-kHz per pass (40-GHz/sec or 1.3-Å/sec) change in source frequency.

The ultimate solution for the minimization of this source of error involves reducing the magnitude of the backscattering itself. A large reduction in the amplitudes of the Rayleigh-scattered waves can be made by using short pulses (perhaps 1 nsec) and gating the output so that only the scattered energy from a short (0.2-m) length of fiber contributes to the part of the

secondary wave that interferes. The short length that matters could be specially processed or constructed to reduce scattering. This, and the equivalent use of frequency modulation and chirp modulation, are the subjects of a forthcoming paper. We believe that improvements in the fiber system and in the modulation process can reduce this source of error to a level less than that which is due to photon noise and other factors.

Discussions with H. Marcatili, M. Chodorow, G. Pavlath, and H. Lefevre have been helpful in developing these concepts.

This work was supported by the U.S. Air Force Office of Scientific Research under contract F49620-80-C-0040.

References

1. V. Vali and R. W. Shorthill, "Fiber ring interferometer," Appl. Opt. **15**, 1099 (1976).
2. D. E. Thompson *et al.*, "Sagnac fiber-ring interferometer gyro with electronic phase sensing using a (GaAl)As laser," Appl. Phys. Lett. **33**, 940 (1978).
3. R. F. Cahill and E. Udd, "Phase-nulling fiber-optic laser gyro," Opt. Lett. **4**, 93 (1979).
4. H. Lefevre, "Optical fiber interferometric gyroscope," Ph.D. thesis (University of Paris, XI-Orsay, 1979).
5. H. Arditty *et al.*, "Recent developments in guided waves optical rotation sensors," in *Digest of Topical Meeting on Integrated and Guided Wave Optics* (Optical Society of America, Washington, D.C., 1980), paper YuC2.
6. W. C. Goss *et al.*, "Fiber-optic rotation sensor technology," Appl. Opt. **19**, 852–858 (1980).
7. R. Ulrich, "Fiber-optic rotation sensing with low drift," Opt. Lett. **5**, 173–175 (1980).
8. H. Arditty *et al.*, "Re-entrant fiber-optic approach to rotation sensing," Proc. Soc. Photo-Opt. Instrum. Eng. **157**, 138 (1978).
9. R. Ulrich and M. Johnson, "Fiber-ring interferometer: polarization analysis," Opt. Lett. **4**, 152 (1979).
10. D. M. Shupe, "Thermally induced nonreciprocity in the fiber-optic interferometer," Appl. Opt. **19**, 654–655 (1980).
11. S. C. Lin and T. G. Giallorenzi, "Sensitivity analysis of the Sagnac-effect, optical fiber ring interferometer," Appl. Opt. **18**, 915 (1979).
12. J. E. Midwinter, *Optical Fibers for Transmission* (Wiley, New York, 1979).